



**Politecnico
di Torino**

Politecnico di Torino

Department of Environment, Land, and Infrastructure Engineering

**Master of Science in Petroleum Engineering
A. y. 2021/2022**

CO₂ INJECTION SIMULATION USING ECLIPS EOR

Supervisor:
Prof. Francesca Verga

Candidate:
Ahmed Zahra

This page intentionally left blank

Abstract

Greenhouse gas emissions are of major worldwide concern nowadays, on top of this list comes CO₂ emissions. There is a global orientation that supports any attempt to reduce carbon emissions, so investigations and research have been developed intensely in this area. One of these attempts is the injection of CO₂ in an oil reservoir to increase its recovery.

Miscible CO₂ injection is an efficient process for increasing enhanced oil recovery (EOR) in oil reservoirs, which has been around in the oil and gas industry for about 40 years. There are some challenges that may face this technique, like finding an economic CO₂ source or producer, achieving the miscibility pressure for better efficiency, and oil prices.

In this thesis, the Eclipse 300 simulator is used to analyze and compare the continuous CO₂ injection and water alternating CO₂ (WACO₂) injection. Both methods are designed and tested by running multiple simulations, then a sensitivity analysis is made to study the effect of some engineering parameters on the enhanced oil recovery and production parameters. The studied parameters are flood pattern, CO₂ and water injection rates, WAG ratio, and total injected volume. Both techniques are applied to light and medium oil.

A model representing a synthetic reservoir is built using FloGrid software while fluid composition and PVT properties are generated by PVTi software.

This study has shown the workflow for CO₂ and WAG-CO₂ injection processes, and a comparison that serves the goal of more economical oil recovery.

1 Contents

Abstract.....	1
List of Figures.....	4
List of Tables.....	6
List of Equations.....	7
Nomenclature.....	8
1 Introduction.....	9
2 Literature Review.....	12
2.1 Miscibility.....	12
2.1.1 Miscible Fluids Phase Behaviour (Ternary Diagram).....	12
2.1.2 MCM displacement.....	13
2.2 MMP and MME.....	17
2.2.1 Slim-Tube Experiment.....	17
2.2.2 MMP and MME calculation.....	17
2.3 Diffusion and Dispersion.....	21
2.3.1 Diffusion in miscible fluids.....	21
2.3.2 Dispersion in porous media.....	22
2.3.3 Factors affecting dispersion in porous media.....	25
2.4 Relative Permeability.....	29
2.4.1 Oil Swelling (Expansion).....	30
2.4.2 Interfacial Tension reduction.....	31
2.4.3 Oil Viscosity Reduction.....	32
2.4.4 Acid Effect on Rock.....	33
2.5 Capillary Pressure.....	33
2.6 CO ₂ injection EOR process.....	33
2.6.1 A case study from literature.....	34
2.7 CO ₂ injection process design.....	35
2.7.1 Food pattern.....	35
2.7.2 CO ₂ injection rates.....	38
2.7.3 Water injection rate.....	40
2.7.4 WAG ratio.....	41
2.7.5 Total injected CO ₂ volume.....	43
3 Numerical Simulation.....	44
3.1 Problem Statement.....	44
3.2 Reference Case.....	45
3.2.1 Reservoir model.....	45
3.2.2 Grid Selection.....	45
3.2.3 Fluid models.....	46

3.2.4	Equation of State.....	47
3.2.5	Other data.....	48
3.2.6	Injection strategy.....	48
3.3	Reference case results	51
3.4	Sensitivity analysis.....	53
3.5	Results and Discussion	54
3.5.1	The effect of flood pattern	54
3.5.2	Effect of CO ₂ injection rate	55
3.5.3	Effect of water injection rate.....	56
3.5.4	WAG ratio.....	57
3.5.5	Effect of total CO ₂ injected volume	58
4	Conclusion	59
5	References.....	61

List of Figures

Figure 1- Oil demand history and forecast (from IEA [40]).....	9
Figure 2-World oil supply and demand, 1971-2020, (from IEA [44])	10
Figure 3- CO2 emission scenarios (from IEA [40]).....	10
Figure 4- Oil production, reserves and residual. [43]	11
Figure 5- Ternary phase diagram for a system consisting of components A, B, and C which are miscible in all proportions, (from [1] Green & Willhite 1998).....	12
Figure 6-Ternary phase diagram for system consisting of components A, B, and C which have limited solubility, (from [1] Green & Willhite 1998).	13
Figure 7- Pseudoternary diagram, (from [1] Green & Willhite 1998).....	13
Figure 8- Ternary phase diagram for an alcohol displacement process, (from [1] Green & Willhite 1998).	13
Figure 9-Vaporizing gas displacement process on a pseudoternary diagram, development of miscibility, (from [1] Green & Willhite 1998).....	14
Figure 10- High pressure process on a pseudoternary diagram, miscibility does not develop, (from [1] Green & Willhite 1998).	14
Figure 11- Enriched gas (condensate) process on a ternary diagram, (from [1] Green & Willhite 1998).	14
Figure 12- Experimental and simulated densities from contact experiment at 3600 psig, (from [27] Zick 1986).....	15
Figure 13- Comparison of two-phase envelopes for methane/HC and CO2/HC systems, (from [1] Green & Willhite 1998).	15
Figure 14- FCM displacement of a C4/C10 mixture by pure CO2, (from [1] Green & Willhite 1998).	15
Figure 15- Dynamic miscible displacement of a C4/C10 mixture by pure CO2, (from [1] Green & Willhite 1998).	16
Figure 16- Dynamic immiscible displacement of a C4/C10 mixture by pure CO2, (from [1] Green & Willhite 1998).	16
Figure 17- CO2 viscosity vs. Pressure at different temperatures, (from [1] Green & Willhite 1998)..	16
Figure 18- Effect of salinity on CO2 solubility in water at a temperature of 77 °F, (from [1] Green & Willhite 1998).	16
Figure 19- CO2 solubility in fresh water (from Dodds et al and Stalkup, (from [1] Green & Willhite 1998).	16
Figure 20- Slim-tube recovery as a function of solvent enrichment level, (from [1] Green & Willhite 1998).	17
Figure 21- Slim-tube data, (from [1] Green & Willhite 1998).	17
Figure 22- Logic of cell-to-cell flash program (from Metcalfe)	18
Figure 23- 45 degree flow model (from [2] Perkins and Johnston 1963)	22
Figure 24-Range of validity of mechanisms of diffusion and dispersion in unconsolidated random packs of uniform size beads in laminar flow (from [2] Perkins and Johnston 1963).....	22
Figure 25- Porous medium being viewed as a series of mixing tank.(from permink.com)	23
Figure 26- Longitudinal dispersion coefficients for porous media (from [2] Perkins and Johnston 1963).....	23
Figure 27- Transverse diffusion scheme (from [2] Perkins and Johnston 1963).....	24
Figure 28- Transvers dispersion coefficients in porous media from [2] Perkins and Johnston 1963)..	24
Figure 29- Effect of dp/dt on transverse dispersion in turbulent flow (from [2] Perkins and Johnston 1963).....	25
Figure 30- Effect of particle size distribution on dispersion (from [2] Perkins and Johnston 1963)....	26
Figure 31- Approximate effect of particle shape on dispersion (from [2] Perkins and Johnston 1963)26	

Figure 32- Evolution of miscible fingering patterns over time, t (expressed as fractions of breakthrough time, t_b) seen in experiments with different viscosity ratios (M), (from [11] Keable and Jones 2021)	27
Figure 33- Suppression of dispersion resulting from favorable mobility ratios, (from [2] Perkins and Johnston 1963).....	28
Figure 34- Ratio of oil relative permeability in CO ₂ injection to N ₂ injection (A) core C3 (B) core C1 (C) core S1.(from [13] Ghoojani and Bolouri 2011)	30
Figure 35- Swelling factor vs. CO ₂ mole fraction (from [16] Simon and Graue 1965).....	31
Figure 36- Oil relative permeability comparison in CO ₂ and N ₂ injection (A) core C3 (B) core C1 (C) core S1. (from [13] Ghoojani and Bolouri 2011).....	32
Figure 37- Viscosity of CO ₂ -oil mixture at 120 F (from [16] Simon and Graue 1965).....	32
Figure 38- Possible locations for infilling wells, class 1 (green), class 0 (blue), (from [58] Kim et al. 2018).....	36
Figure 39- Concept of boundaries creation in Voronoi diagram (from [58] Kim et al. 2018).....	37
Figure 40- Reservoir divided into regions based on Voronoi diagram (from [58] Kim et al. 2018)	37
Figure 41- From [46] Perera and Gamage 2016	38
Figure 42- From [46] Perera and Gamage 2016	39
Figure 43- from [59] Kaita and Ogolo 2020	39
Figure 44- from [59] Kaita and Ogolo 2020	40
Figure 45- from [60] Ghoojani and Bolouri 2012.....	40
Figure 46- From [46] Perera and Gamage 2016	41
Figure 47-From [46] Perera and Gamage 2016	42
Figure 48- from [56] Yang and Song 2015.....	43
Figure 49- Oil recovery factor vs. total injected CO ₂ in terms of HCPV (from [65] Saman and Curtis (2014))	43
Figure 50- From [46] Perera and Gamage 2016	44
Figure 51- Grid model	46
Figure 52- Well pattern in reference case	48
Figure 53- Flow chart of the process strategy.....	50
Figure 54- Recovery facrot after 23 years simulation time, WAG region (green), CO ₂ region (blue) (LGT_OIL)	51
Figure 55- Reference case field water cut (LGT_OIL).....	51
Figure 56- Reference case water production, WAG region (green), and CO ₂ region (blue) (LGT_OIL)	51
Figure 57- Reference case field GOR (LGT_OIL)	52
Figure 58- Reference filed recovery factors, WAG region (green), CO ₂ region (blue), (medium oil) 52	52
Figure 59- Reference field water cut (medium oil).....	53
Figure 60- Reference field water production, WAG region (green), CO ₂ region (blue), (medium oil)	53
Figure 61- Reference filed GOR (medium oil)	53
Figure 63- Contiuous CO ₂ region recovery factors (light oil).....	55
Figure 62- WAG region recovery factors (light oil)	55
Figure 65- GOR in continuous CO ₂ region.....	55
Figure 67- Field GOR for different CO ₂ injection rates (light oil).....	56
Figure 66- Field recovery factors for different CO ₂ injection rates (light oil)	56
Figure 68-Water injection rates in WAG region (light oil).....	57
Figure 69- Recovery factor in WAG region with different WAG ratios (light oil).....	58
Figure 70- Effect of total injected volume of CO ₂ on the recovery factor, contiuuous CO ₂ region (light oil)	59

List of Tables

Table 1- Best fit coefficients for pure CO ₂ MMP correlation (from [38] Yuan and Johns 2004).....	21
Table 2-Effect of CO ₂ and N ₂ on IFT, oil viscosity and swelling factor (from [13] Ghoojani and Bolouri 2011).....	29
Table 3- Criteria of applicability of miscible CO ₂ EOR process (from [67] Shaw and Bachu 2016)..	34
Table 4 – Reservoir model data	45
Table 5 - Fluids composition and fractions.....	46
Table 6 - Oil properties	46
Table 7- Sensitivity analysis strategy.....	54
Table 8- Key legend of the well patern simulation figures	54
Table 9- Key legend for the effect of CO ₂ inj. rate figures	56
Table 10- Key legend for water injection rates	57
Table 11- Key legend for figure 69.....	57
Table 12- Key legend for figure 70.....	58

List of Equations

Equation 1- MMP correlation for pure CO ₂ injection (from Yuan and Johns)	20
Equation 2. Fick's diffusion equation.....	21
Equation 3. Fick's extended equation.....	22
Equation 4- Diffusion - Formation Resistivity Factor relation	22
Equation 5- Raimondi, et al, equation.....	23
Equation 6- Total longitudinal dispersion equation	24
Equation 7-Total transverse dispersion equation	24
Equation 8- Singer and Wilhelm correction for wall effect.....	25
Equation 9- Particle size distribution slope equation.....	26
Equation 10- Peclet number equation	28
Equation 11- Fracture pressure equation	48

Nomenclature

IFT	Interfacial Tension
FCM	First Contact Miscibility
MCM	Multiple Contact Miscibility
LPG	Liquefied Petroleum Gas
WAG	Water Alternating Gas
Ed	Displacement Efficiency
Sor	Residual Oil Saturation
MMP	Minimum Miscibility Pressure
MME	Minimum Miscibility Enrichment
HC	Hydrocarbon
D	Apparent Diffusion Coefficient in a Porous Medium
Do	Molecular Diffusion Coefficient
F	Formation Electrical Resistivity Factor
Φ	Porosity
C	Concentration
Ψ	Sphericity
FVF	Formation Volume Factor
KL	Longitudinal Dispersion Coefficient
Kt	Total Dispersion Coefficient
E	Convective Dispersion Coefficient
U	Average Velocity
dp	Particle Diameter
σ	Heterogeneity Parameter
M	Mobility Ratio
μ	Viscosity
q	Flow Rate
A	Cross-Sectional Area
Pp	Pore Pressure
Pfr	Fracture Pressure
Pov	Overburden Pressure
K	Matrix Stress Coefficient

1 Introduction

For decades, oil has been a dominant source of energy in constructing our modern civilization. In addition, it is the main resource in the petrochemical industry, the products of which are critically present in our everyday life. The slope of the annual incremental oil production is decreasing in the latest years, and it is about time until this annual increment turns into a reduction. [42] If this reduction continues, the gap between the oil supply and the increasing energy demand will continue increasing (Fig 2), in other words, the global oil supply will be much lower than the global demand. With the international orientation toward net zero GHG emissions by 2050, there is a hope of overcoming the predicted risk of oil production insufficiency. [40] [41] This risk could also be mitigated by increasing oil production, a report done by the United States Department of Energy, explains in detail how is it possible that CO2 EOR could be the perfect way to achieve higher production with lower emissions. [43]

The next two figures can explain the situation, Fig 1 shows the predicted demand in different scenarios. Fig 2 shows the increasing gap between oil and NGL supply and demand.

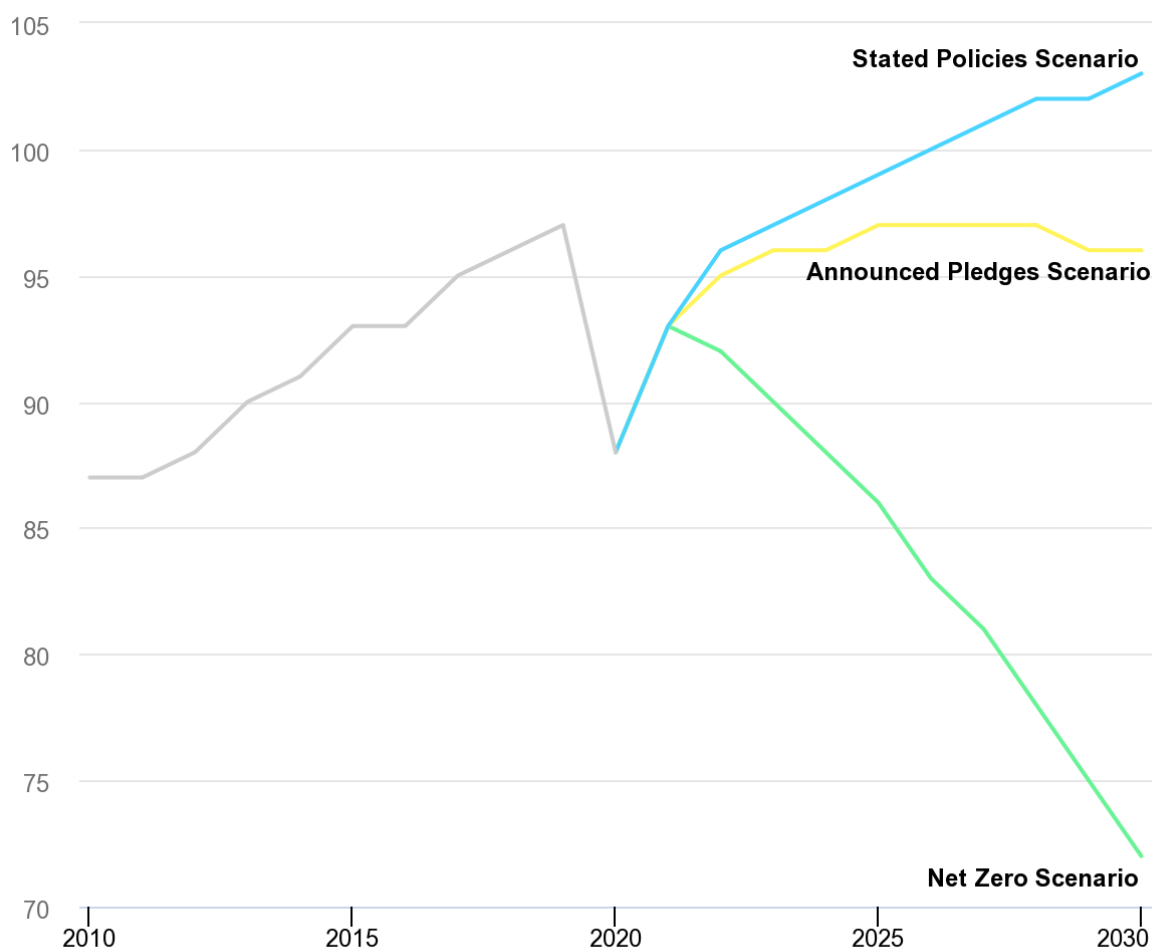


Figure 1- Oil demand history and forecast (from IEA [40])

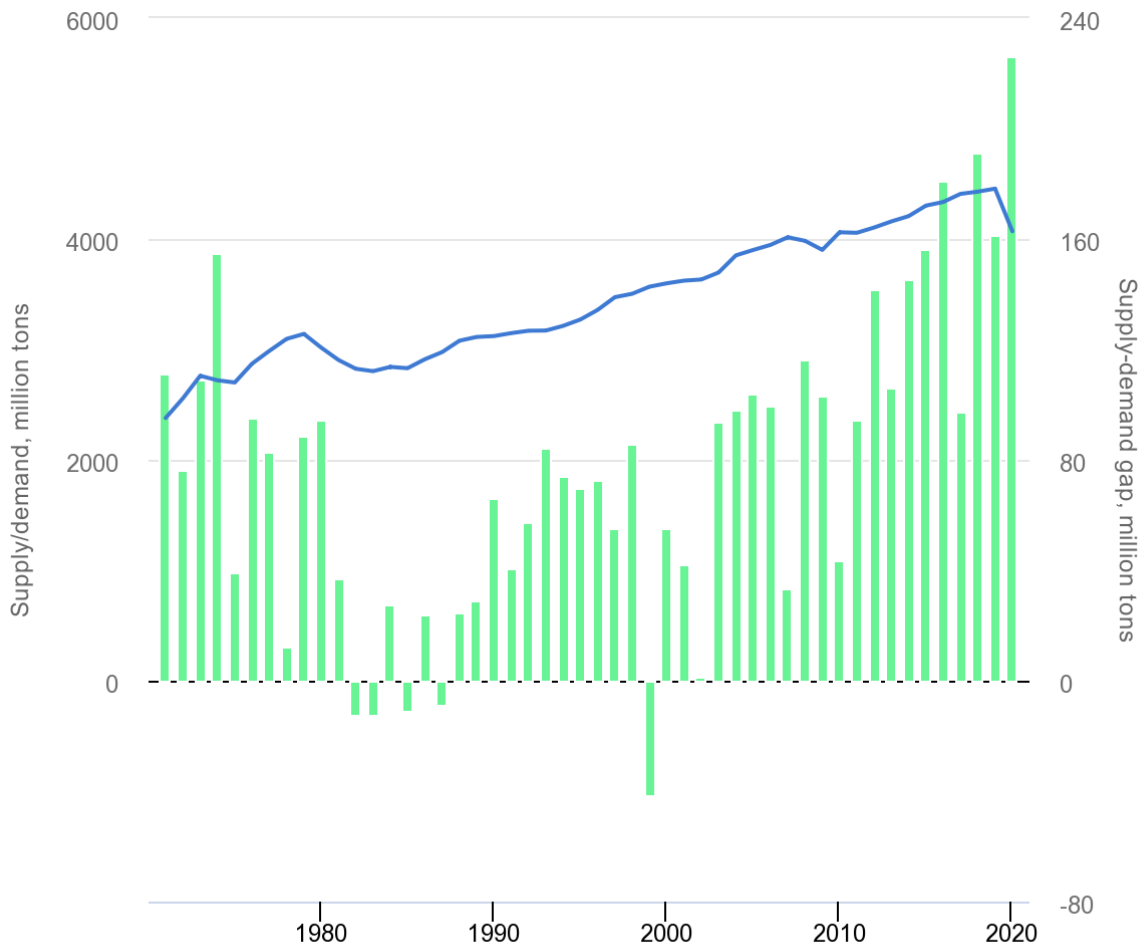


Figure 2-World oil supply and demand, 1971-2020, (from IEA [44])

The real challenge is not only to find a way to increase and sustain oil production for the longest possible period but also to decrease GHG emissions to the lowest. IEA has made a detailed report that includes possible upcoming scenarios that may happen and the possible consequences, the report also consists of a realistic plan of consumption reduction in each industrial sector along with recommendations for the critical industries where the application of carbon capture will be most effective to reach this goal. [41]

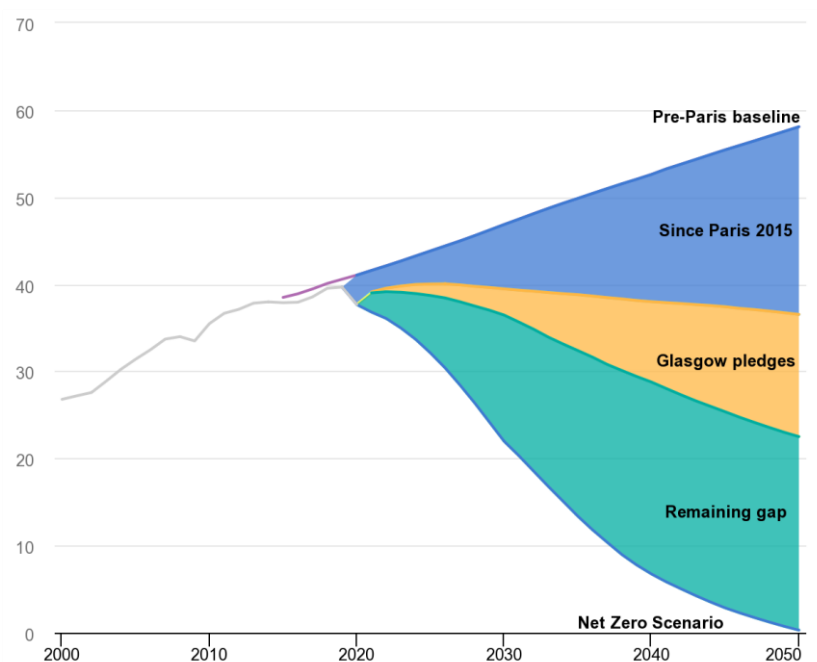


Figure 3- CO2 emission scenarios (from IEA [40])

The US Department of Energy report estimated the producible oil after primary and secondary recovery by 33% while the remaining oil represents 67% of the original oil in place. [43]

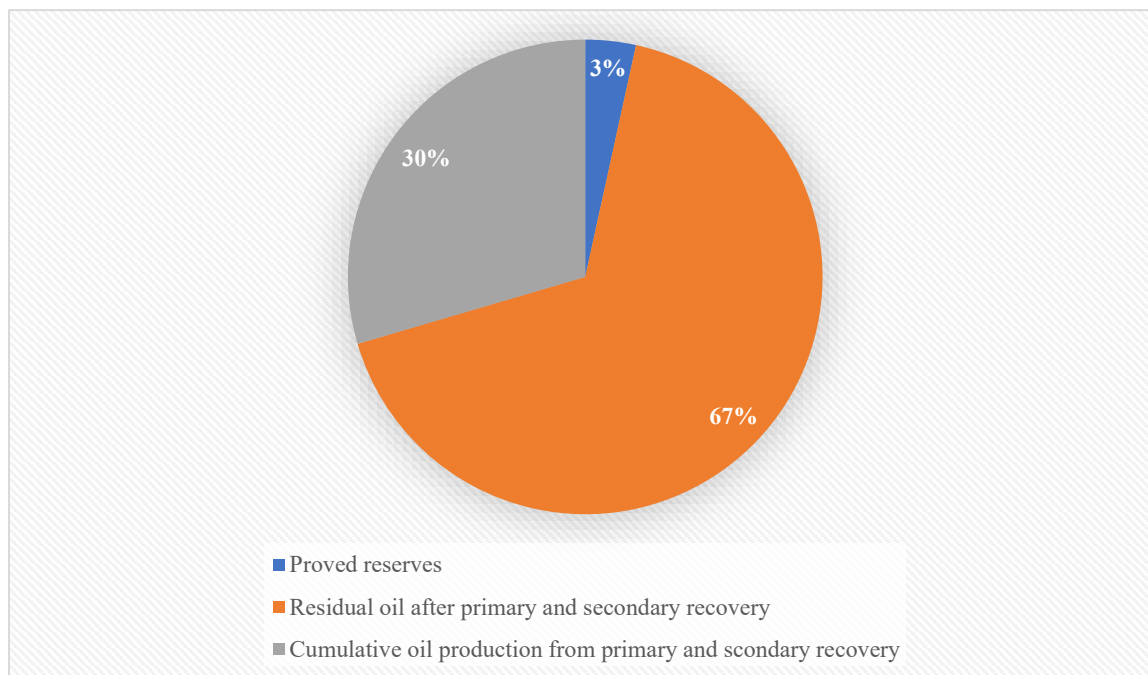


Figure 4- Oil production, reserves and residual. [43]

According to an investigation done by Hook and Hirsch, the so-called "giant oil fields" are the bedrock of world oil production. Their analysis reveals the declining trends of production rates that giant fields have been following in the latest years. With more giant fields entering the production declination period, and fewer giant fields being discovered, there is an urge to prioritize giant fields for future development. [42]

Green and Willhite have explained, in great detail, different EOR processes, one of which is CO₂ injection. Reservoir oil mobility is significantly increased upon miscible mixing with CO₂, leading to production enhancement. [1]

CO₂ injection has been used commercially as an effective EOR technique since 1972 in the USA, Permian Basin. [48] In 2018, CO₂ EOR was utilized in more than 160 projects worldwide, with total oil production increments of about 350,000 bpd. [47] The application of this EOR technique in the US was aided by a strong infrastructure of pipelines network to transport CO₂, along with the availability of cost-effective CO₂ suppliers. That's why it hasn't been applied outside the US on a significant scale until about 17 years ago. [46] Nowadays, CO₂ injection is the second globally used EOR technique, after thermal recovery, in medium oil production. [45]

CO₂ is indeed an efficient way for EOR under the right circumstances, the most important of which is cost. Generally, commercial CO₂ EOR projects use naturally occurring CO₂, which is relatively cheap. However, the project will not be environmentally friendly unless the source of CO₂ is anthropological. [46] Research in carbon capture and utilization has yielded promising results, anthropological CO₂ has been used in Weyburn CO₂ EOR project in Canada. A huge demonstration project in which a successful attempt of CO₂ capturing, using in EOR, and storing. [49]

The target of this thesis is to investigate EOR by injection of miscible CO₂ and the associated factors that may lead to better oil recovery. This will be done by presenting a study about the process of miscible CO₂ - EOR, numerical modeling, and a literature review about related concepts, mechanisms, interactions, and effective parameters.

2 Literature Review

2.1 Miscibility

Total miscibility is the absence of IFT between fluids; therefore there are no capillary forces. So ideally no oil droplets are trapped ($S_{or}=0$). Generally, miscible displacement has high displacement efficiency (E_d). In immiscible injection, like Waterflooding, the injected water traps and isolates oil droplets, and they cannot flow due to IFT which results in an appreciable value of capillary forces.

There are two types of miscibility:

- FCM: A process of injection of a displacing fluid (i.e.: butane) which forms a single phase and mixes in all proportions with the oil upon first contact.
- MCM: A process of injection of a displacing fluid (i.e.: CO₂) which undergoes mass transfer with the oil in place resulting in a compositional alteration of both the injected solvent and the oil leading to miscibility between the two fluids.

Ideally, if we use a fluid like LPG to apply the FCM displacement process we will obtain a 100% E_d . In practice, solvents that are miscible with oil are more expensive than water and dry gas, which are immiscible, so injected slug must be relatively small for economic considerations.

Therefore, just after primary miscible gas, we may employ a chase fluid or a secondary fluid, a less expensive slug (lean gas, water, nitrogen, or air) which might not be a very effective solvent itself but should be miscible with the main slug. [1]

2.1.1 Miscible Fluids Phase Behaviour (Ternary Diagram)

There are various ways to represent phase behavior, including Ternary Diagram, Single Phase Isothermal P-V Diagram, Pressure Composition Diagram, Constant Composition Pressure-Temperature Phase Diagram, and Binary Phase Isothermal Phase Diagram.

The ternary or triangular phase diagram is a useful way to describe the phase behavior, in a displacement process, at the contact zone of liquid/liquid or vapor/liquid equilibrium. It describes the composition of an isobaric and isothermal three-component system, if the system has more components, then they are grouped into three groups. A common way to represent crude oil is to decompose it into CH₄, C₂-C₆, and C₇+. It describes composition using the percentage of either weight, mole, or volume. It should be noted that if volume percent is used there shouldn't be any significant change in volume with mixing.

An equilateral triangle is used, vertexes represent pure components or groups, sides represent binary components or groups, and points interior to the triangle represent the three-component system. If the three components are miscible, multiphase regions will not appear in the diagram. The component concentration is represented by the perpendicular distance from the point P to the opposite baseline. Concentrations are represented by the ratio between these distances. The sum of these distances equals the triangle altitude, so we can refer to this when calculating the ratio.

A property of the ternary diagram (Fig 5), if we start with the mixture M (binary mixture A-C) and then add gradually component B, all ternary mixtures of the binary mixture M will lie on the line BM. [1]

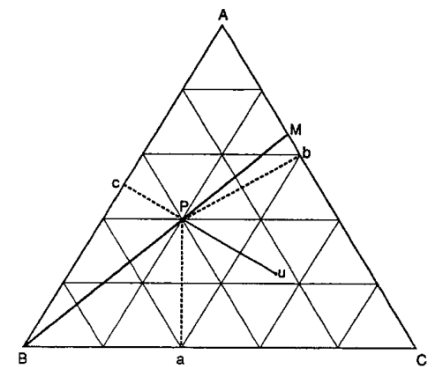


Figure 5- Ternary phase diagram for a system consisting of components A, B, and C which are miscible in all proportions, (from [1] Green & Willhite 1998).

Inverse-lever-arm rule: $MP/MB = \text{the amount of component B} / \text{the total amount}$.

The same rules always apply, for example, if a mixture U is added to mixture P, all possible mixtures of U and P lie on the line PU, and the final mixture will be determined by the Inverse-lever-arm rule.

The binodal curve, in (Fig 6), is the two-phase envelope of the ternary diagram. Point P represents the overall composition of a mixture inside the binodal curve. This means the two phases, liquid, and gas, are not miscible and are separated into a liquid and a gas phase. The composition of the liquid phase is represented by point X located on the curve and shifted towards the heavier component C. While point Y represents gas composition. The line XY passes through P where the rule of “Inverted-lever-arm” applies to identify the percentage of each phase (not component). .

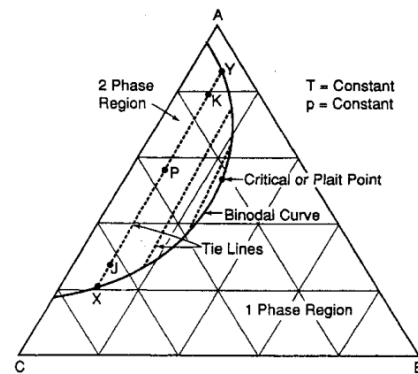


Figure 6-Ternary phase diagram for system consisting of components A, B, and C which have limited solubility, (from [1] Green & Willhite 1998).

Lines connecting equilibrium concentrations like XY are called tie-lines, there are infinite numbers of these lines because there are infinite possible concentrations inside the binodal curve, but only several lines are represented and the others are interpolated. The endpoints of the tie-lines converge towards the critical point or the “plait” point, where the phase properties are indistinguishable at the specified P and T. IFT between phases at the vicinity of the “plait” point approaches zero. Along each tie-line, the concentration of each component changes overall so as the phase percentage, K has more gas and J has more liquid, but the concentration of components in the phase itself does not change, X and Y have the same component ratio along the line but the amount of X and Y changes.

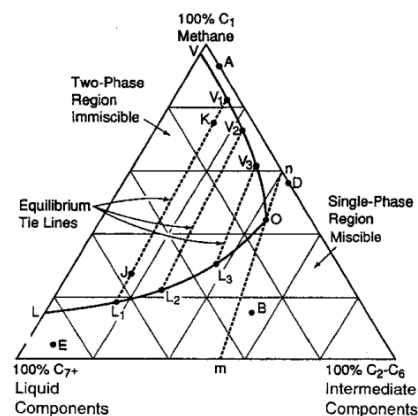


Figure 7- Pseudoternary diagram, (from [1] Green & Willhite 1998).

When hydrocarbons are involved, we use a pseudo-ternary diagram (Fig 7), where we represent them by separating the many unidentifiable components into groups or pseudo-components.

An important assumption is the composition of a pseudo-component does not change in any phase. Phase boundary VO is the saturated vapor curve and BO is the saturated liquid curve, intersecting at the critical point O.

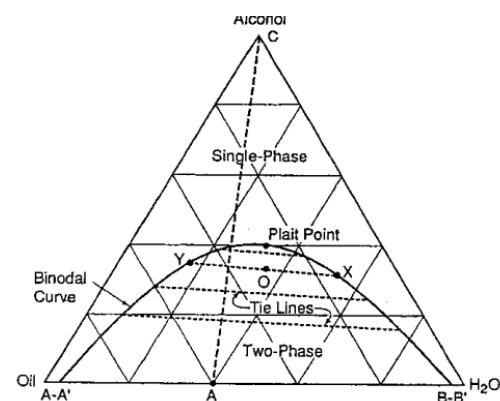


Figure 8- Ternary phase diagram for an alcohol displacement process, (from [1] Green & Willhite 1998).

The pseudo-ternary diagram can also describe a three-component system of Oil-Water-Alcohol (Fig 8). Any point under the binodal curve represents a system of two-phase, point O has a water-rich phase X and an oil-rich phase Y. Both are in equilibrium but separated by IFT. Distance AA' represents the solubility of water in oil, as this is the maximum distance (percentage) water can exist with oil in one phase. Alcohol is soluble in both oil and water.

Alcohol can displace both oil and water without leaving any residual oil, it is only done in the lab due to economic and technical reasons. They will be all in one phase above the binodal curve, where oil and water are both solubilized in alcohol. [1]

2.1.2 MCM displacement

MCM can be classified into:

- Vaporizing gas (lean gas) displacement
- Condensing and Condensing/Vaporizing gas (enriched gas) displacement
- CO₂ miscible displacement

2.1.2.1 Vaporizing gas displacement

Lean gas contains mostly methane CH₄ and other low MW hydrocarbons, sometimes it contains some inert gases like Nitrogen. During this process, intermediate components will evaporate from the reservoir oil enriching the injected gas through multiple contacts. Under the proper conditions, at some point, the enriched gas will become miscible with the reservoir oil.

The process of enrichment is described by the ternary diagram (Fig 9), gas A is injected into the reservoir with oil C, and change in the composition will follow the line AC, we reach an overall composition “a” with enriched gas-phase V₁ and liquid phase L₁, with continues movement (multiple contacts), V₁ will mix once again with oil C, following the line CV₁ reaching “b” and so on, until we reach final composition at the interface between the injected gas and the reservoir oil at point “e” outside the binodal curve, which means there are finally acting as one phase, the became miscible. The process is described in reservoir P and T. Thermodynamic equilibrium is assumed since the flow rates are too low in the reservoir, except in the vicinity of the wellbore.

An example of miscibility failure is in Fig 10, whereby spending some time injecting gas A, we reached point “c” with gas-phase V₃ which is aligned with oil B through its tie-line, this means by further contact, there will be no further change in composition. The distinction between the processes that will be miscible or immiscible is separated by what so-called, Limiting tie line, a tangent line to the “plait” point.

Generally, if we increase pressure the binodal curve shrinks. The minimum pressure (MMP) at which the Injected slug is miscible with the reservoir oil. The MMP in the MCM process is the minimum pressure at which it is possible to develop miscibility between the injection slug and the reservoir oil.

[1]

2.1.2.2 Condensing and Condensing/Vaporizing gas displacement

Enriched gas is a gas with a significant amount of intermediate components (C₂-C₆). The **condensing** process depends on condensing these components into the oil to change its composition to become miscible with the Injected gas. Typically, this process is operated under lower pressure than the Vaporizing process. Fig 11 describes the condensation of injected gas A into reservoir oil C. The figure focuses on the composition change of the oil so lines are drawn between L_n and the Injected gas A. It should be noted that miscibility will eventually develop because gas composition A is at the right-hand side of the limiting tie line.

The MMP for condensing the MCM process is the minimum pressure

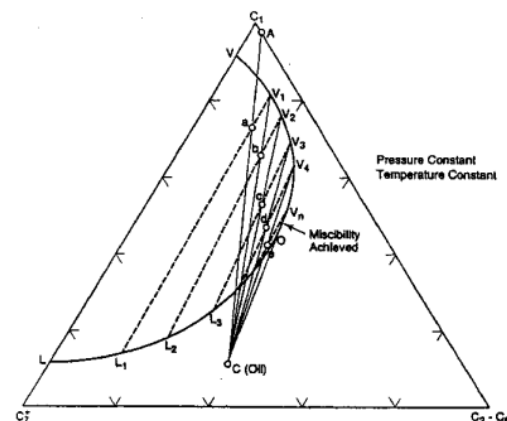


Figure 9-Vaporizing gas displacement process on a pseudoternary diagram, development of miscibility, (from [1] Green & Willhite 1998).

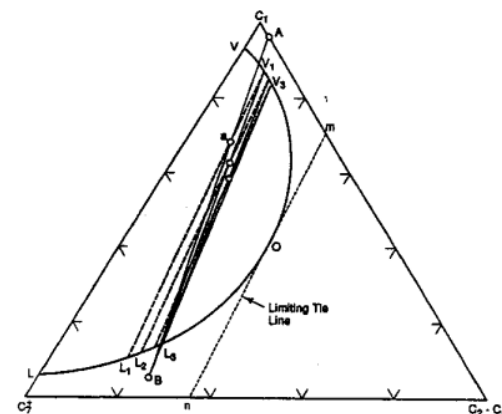


Figure 10- High pressure process on a pseudoternary diagram, miscibility does not develop, (from [1] Green & Willhite 1998).

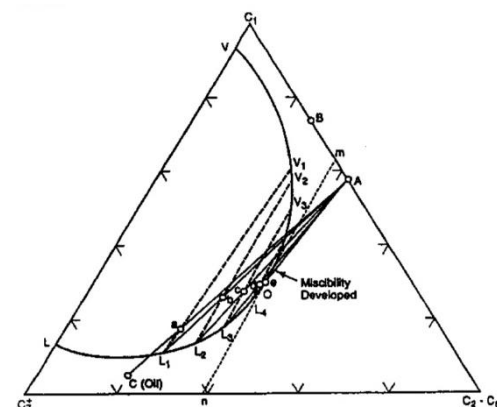


Figure 11- Enriched gas (condensate) process on a ternary diagram, (from [1] Green & Willhite 1998).

at which the limiting tie line just passes through the Injected slug composition A. This will make point A at the right and point C at the left with the limiting tie line.

If point A at the left and point C is right, this is a lean gas injection and miscibility is reachable. If the two points, A (gas) and C (oil), are on the right-hand side then they are already soluble in each other. If both points are on the left side, the two fluids will maintain immiscibility, unless it is applicable to increase the pressure leading the binodal curve to shrink and the limiting tie line to move left until one of the points become on the right side.

In practice, it is found that it is a condensation/vaporization process. What really happens besides the condensation of lower intermediates (C2-C4) to the oil, is the vaporization of higher intermediates (C4+) from the oil into the Injected gas. This behavior makes the oil becomes heavier especially in the vicinity of the injection well, where the Injected gas with higher mobility bypasses the contacted oil stripping it from the higher intermediates.

Over time oil near-wellbore will become saturated with the condensed lower intermediates. Further contact with the newly injected gas will not lead to further condensation, however, it will continue stripping higher intermediates from the oil. This leads to a very rich gas at depth from the wellbore and medium oil near the wellbore.

To a certain extent, this very rich gas will become "nearly" miscible with the original reservoir oil. However, miscibility is not reached in all proportions, as the gas is "nearly" not totally miscible (a single-phase may never be reached), however, an efficient displacement can take place. [1]

Zick (1986) proved that it is a condensation/vaporization process through multiple contacts between enriched gas and oil in a PVT cell, then by measuring densities, gas density was increased where it was supposed to decline if it was only condensation of higher MW (relatively to methane) into the oil. Oil density declined first due to condensing lower intermediates then started increasing due to stripping (Fig 12). [27]

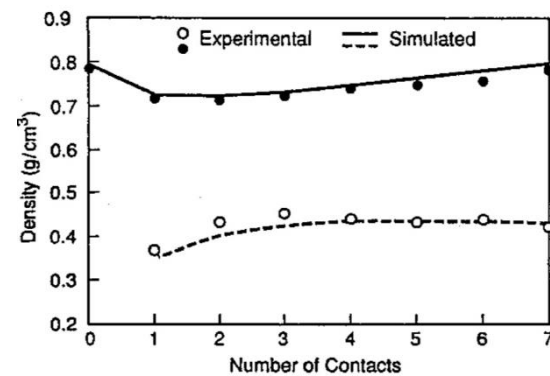


Figure 12- Experimental and simulated densities from contact experiment at 3600 psig, (from [27] Zick 1986).

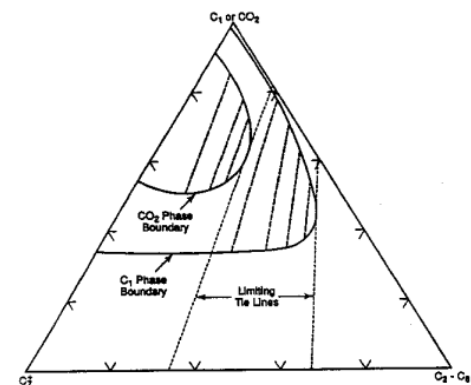


Figure 13- Comparison of two-phase envelopes for methane/HC and CO2/HC systems, (from [1] Green & Willhite 1998).

Another issue is that the pseudo-ternary diagram may not be a true way to represent the pseudo components, because in the condensation/vaporization process we have subcomponents from a pseudo-component that do not partition in the different phases in the same proportions as assumed in the usage of pseudo ternary. If the process was only condensation pseudo ternary will be good enough to represent the process. [1]

2.1.2.3 CO₂ Miscible displacement

The process of CO₂ miscible displacement is similar to the vaporization process except it needs a lower pressure so, at the same pressure and temperature, we see a smaller two-phase region (Fig 13) which represents CO₂.

In addition, the limiting tie line in the case of CO₂ tends to be more parallel to the CO₂-C₇₊ side, giving a better possibility for an oil to be miscible and allowing miscibility to be developed at a lower reservoir pressure than methane.

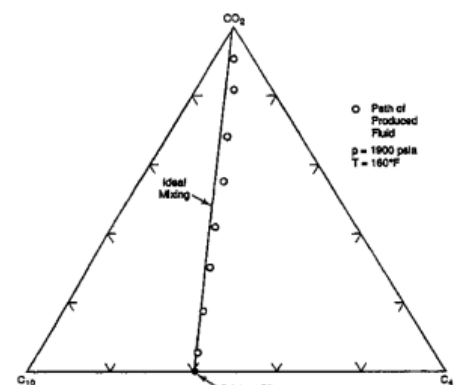


Figure 14- FCM displacement of a C₄/C₁₀ mixture by pure CO₂, (from [1] Green & Willhite 1998).

Metcalf and Yarborough applied an experiment to define the role of phase behavior in miscible displacement. A sandstone core at 160 °F and 1900 psi, the system is C₄ and C₁₀

oil displaced by CO₂ in injection. At these conditions (Fig 14), the process is FCM and the efficiency is 99%. At 1700 psi the process is MCM as Fig 15 shows and the efficiency is 90%. Efficiency decreases because miscibility is not developed in all proportions whereas in some "miscibility zones", miscibility is lost temporarily or permanently.

At 1500 there is no miscibility and the efficiency is 81% (Fig 16). [1]

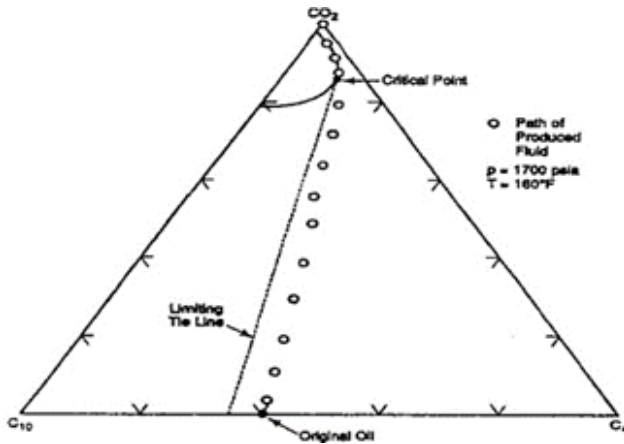


Figure 15- Dynamic miscible displacement of a C₄/C₁₀ mixture by pure CO₂, (from [1] Green & Willhite 1998).

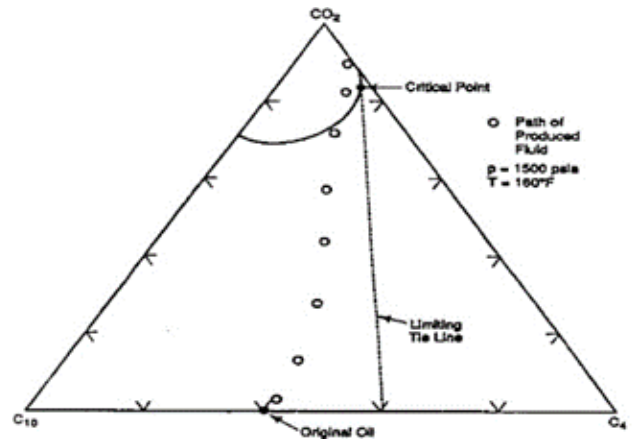


Figure 16- Dynamic immiscible displacement of a C₄/C₁₀ mixture by pure CO₂, (from [1] Green & Willhite 1998).

For calculating the loss of CO₂ in water by solubility, charts are used. From the formation volume factors, 370 SCM of CO₂ is required to fill one cubic meter of reservoir volume, whereas only 140 SCM of air is required at the same temperature and pressure. Thus about three times as many moles of CO₂ are required to fill the same reservoir volume as air.

CO₂ viscosity is generally two or three times higher than the viscosities of CH₄, air, flue gas, and N₂. Relative to a hydrocarbon liquid or water viscosity, the values are still low. However, the CO₂/oil mobility ratio will be two or three times smaller than the other light solvents; hence volumetric sweep efficiency will generally be better for CO₂. [1]

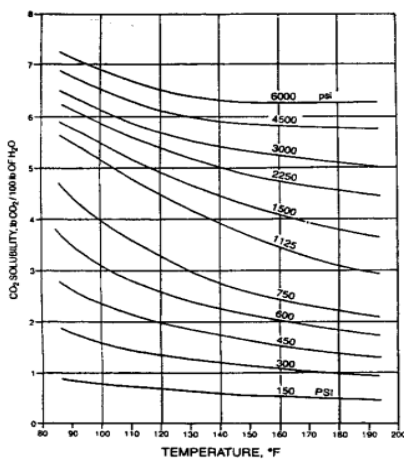


Figure 19- CO₂ solubility in fresh water (from Dodds et al and Stalkup, (from [1] Green & Willhite 1998).

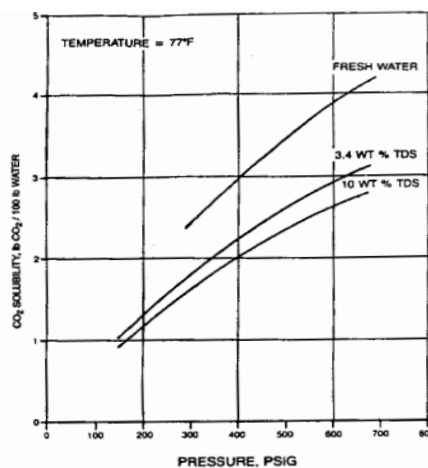


Figure 18- Effect of salinity on CO₂ solubility in water at a temperature of 77 °F, (from [1] Green & Willhite 1998).

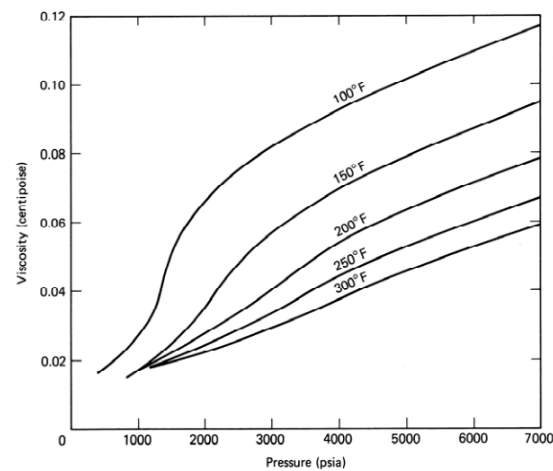


Figure 17- CO₂ viscosity vs. Pressure at different temperatures, (from [1] Green & Willhite 1998).

2.2 MMP and MME

2.2.1 Slim-Tube Experiment

Slim-tube test is a laboratory experiment that estimates the MMP or MMC of a solvent with oil. A long coiled tube filled with sand to simulate a porous medium. Each test starts with saturating the tube with oil at the reservoir temperature, then gas is injected. After 1.2 pore-volumes is injected, the final oil recovery is recorded. Composition, density, and effluent production are measured and recorded as with the injected solvent volume under different pressures. Slim tube test results are identification of MMP or MME (Fig 20 and 21), we take the value that corresponds to a “break” where a further increase of pressure will add very little increase in the recovery factor.

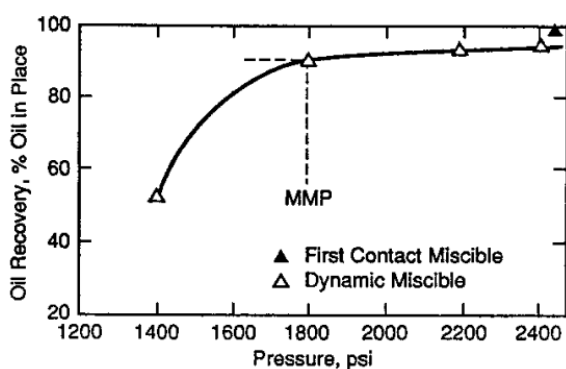


Figure 21- Slim-tube data, (from [1] Green & Willhite 1998).

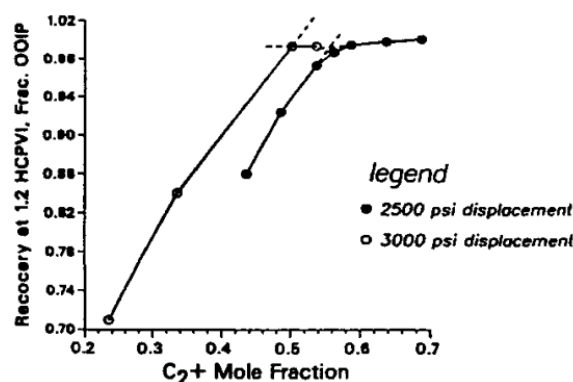


Figure 20- Slim-tube recovery as a function of solvent enrichment level, (from [1] Green & Willhite 1998).

2.2.2 MMP and MME calculation

Several investigators have proposed various calculation methods for MMP and MME, the earliest ones were based on the MCM ternary theory. [21]

In 1959, Benham et al. calculated MME in a condensing gas miscibility system using tie lines extension. The proposed correlation and calculation method are a starting point for laboratory tests, and helpful in the field preliminary evaluation of enriched gas injection EOR processes. He stated that the development of miscibility between reservoir oil and injected enriched gas is favored by high pressure, low temperature, light oil, and gas rich in heavier components. [22]

In 1973, Metcalfe et al. proposed another simple and cheap model (Fig 22) that could be used to describe miscibility development by condensing between reservoir oil and enriched gas in an MCM process. The method comprises of injection of gas in a cell full of oil under certain pressure and temperature, the mixture is then flashed and the excess volume of oil and vapor goes to the next cell then the process is repeated several times. The pressure that produces a mixture in the vicinity of the critical line was defined as the MMP. [23]

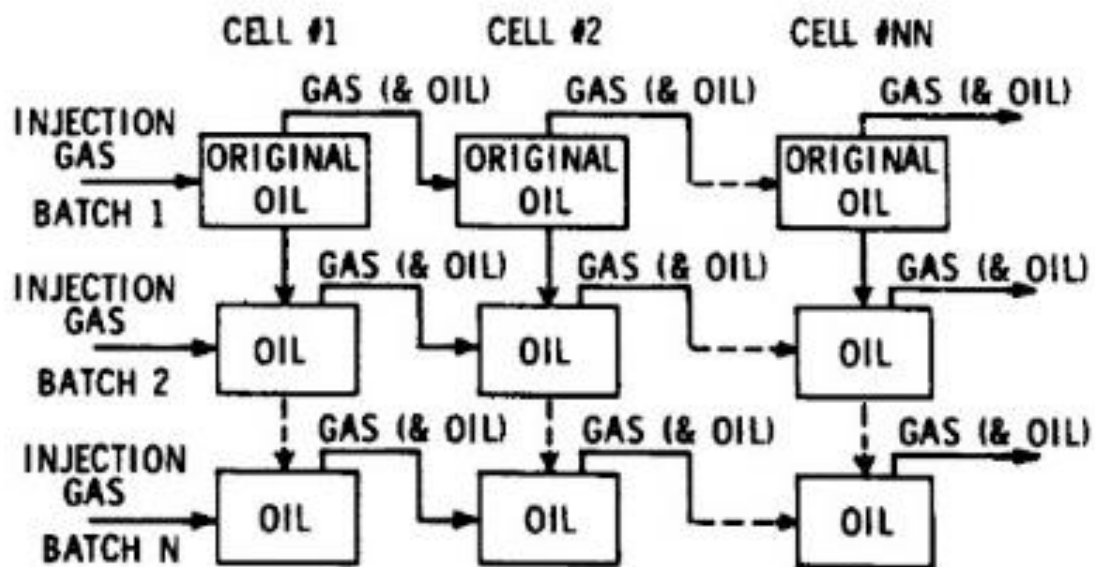


Figure 22- Logic of cell-to-cell flash program (from Metcalfe)

In 1985, Kue attempted to calculate the MMP of CO₂ and enriched gas with reservoir oil in a condensing gas displacement system using the mixing cell approach. However, he used a different version of the model built by Metcalfe, he used a single-cell model. The gas is mixed with the oil that fills the cell then the mixture is flashed. The vapor is removed and a new patch of the injection gas is mixed with the oil in the cell. This process is repeated until the composition of the oil converges to a critical mixture, where liquid and vapor intrinsic properties become identical, and the mixture is considered miscible. If the oil composition does not approach the critical composition, pressure increases until it does, and MMP is found. Based on this process, Kue also proposed a correlation that may be used to calculate the MME if pressure, temperature, and compositions are known. This correlation is only valid in a certain range of pressures, temperatures, and fluid composition, however, it is better than Benham's as it is valid in a wider range of compositions. [24] In 1987, Luks et al. followed the same attempt for vaporizing and condensing gas drive systems. [25]

In 1986, Nouar and Flock proposed a different method for the calculation of MMP from the ternary diagram properties. The method is developed for a three-component system with vaporizing gas drive by lean gas. The idea is based on defining the oil composition and representing it on the ternary diagram, then at a certain pressure, the critical line is drawn. If the point that represents oil composition is at the left-hand side of the critical tie line (the same side of lean gas) the mixture is considered immiscible then pressure is increased. Until a certain pressure is reached where the critical tie line intersects the point that represents oil composition, this pressure is taken as the MMP. The authors proved that this method can be also extended to the condensing gas drive. They used the Soave-Redlich-Kwong equation of state in the development of this method, however, they stated that results accuracy can improve if a more accurate EOS is used. [26]

Extension of these three component system methods to serve a multi-component system needs more information about the system. [20] In practice, condensing gas drive is always accompanied by vaporizing gas drive, this was proven by Zick in 1986 and confirmed by Stalkup in 1987. When condensing/vaporizing mechanism is dominant, the pseudo-ternary diagram is totally not accurate at forecasting miscible displacement of the enriched gas-oil mixture due to the residual oil that is actually found but not predicted. Otherwise, MMP can be determined by one-dimensional compositional simulation. However, it is affected by numerical dispersion that is highly obvious in the

field scale and requires correction. [27][28] Dispersion, both numerical and physical, is more severe when enriched gas is driven with water. This causes a deviation in MME towards higher values. [28] In 1990 Jensen and Michelsen also concluded the inefficiency of the critical tie line method to predict MMP. Instead, they supported the mixing cell theory, using multi-cell models and avoiding the single-cell method because the latter is misleading in MMP prediction. [29]

In 1990 Monroe et al. demonstrated there are three key tie lines that control the miscibility development, the one that extends through the oil composition point, the one that extends through the injected gas composition point, and a tie line called "the crossover tie line". [30] If one of these three key tie lines is the critical tie line MCM develops. In most of the reported cases, the crossover tie line is the tie line that controls the process of miscibility development, where the crossover tie line approaches the critical tie line when the MMP is reached. [31]

In the vaporizing mechanism, the gas tie line is in control, because the gas composition is the one that is changing as it is being enriched. On the other hand. In condensing mechanism, the oil tie line is the one in control, as the oil composition is changing and it becomes lighter at the gas oil interface. While in the condensing-vaporizing mechanism, the crossover tie line controls miscibility, because both gas and oil compositions are changing. [32] When the crossover tie line is in control, condensing/vaporizing mechanism dominants and methods that depend on the oil or injected gas tie line to define miscibility development are not descriptive. Thus, the relationship between the critical tie line and either injected gas composition or initial oil composition is not accurate in defining MMP. [32] This is why critical tie line and single-cell methods are not accurate and are disapproved by Zick, Stalkup, and Jensen. [20]

In 1996, Johns and Orr applied the analytical approach to three, four, five, and eleven-component systems to study MCM displacement. The analytical solution calculates the propagation velocity of a defined mixture composition in a porous medium, based on the method of characteristics (MOC). For miscibility to develop, a unique route between initial oil and injected gas should represent the composition route. This route is governed by three "constraints": velocity constraints, entropy conditions, and continuity conditions. Velocity constraints decide if changing from a certain path or direction to another is valid or not. If this constraint is violated, and it is usually done, a displacement shock is created. [33] When a shock connects two tie lines, an intersection should happen upon their extension. [32]

In the CO₂-C₁-C₄-C₁₀ system that they considered, shocks have contacted the three key tie lines. The crossover tie line intersects the extension of the other two. They concluded that in the presence of a gas cap, MCM is allowed to happen normally. In a CO₂-oil system, the dominant displacement mechanism is condensing-vaporizing, and the key tie line is a crossover tie line that is most downstream. While in N₂-oil or C₁-oil systems, the dominant displacement mechanism is vaporizing, therefore the key tie line is the oil tie line. [33]

In 1997, Wang and Orr used a modified negative flash calculation to solve for the key tie line intersection points and get the MMP. They stated that displacement in an MCM process of liquid oil by a single component injected gas can be represented by a flash calculation applied on a monophasic multicomponent system where the tie line intersection point represents composition. They manipulated the standard flash equation and concluded a modified flash equation that is capable of predicting the key tie line that controls the process, by increasing pressure and finding which one of them converges to the critical point. Then MMP is revealed upon calculation of controlling key tie line length. As the pressure increases, the controlling tie line approaches the plait point and its length reduces. MMP is defined at a length equal to zero. These investigators applied the previous calculations to two systems, one-component injection gas with a multicomponent oil and bi-component injection gas with a four-component oil. [34]

In 2000, Wang and Franklin utilized the tie line intersection approach to forecasting precise values for MMP in more complicated systems. They used systems of injection gas and oil both initially comprising multi-components. The key tie lines here are a little bit different from before, the crossover tie lines are no more one line but it is a set of lines as a result of the injection of

multicomponent gas, their number is $N_c - 3$, where N_c is the number of components in the injected gas. The MMP is still defined at the zero-length key tie line. This method of MMP calculation is valid for checking the precision at which a fluid characterization can regenerate the slim tube results. [20]

MMP can be defined by four techniques: laboratory measurement, numerical simulation, numerical calculation, and analytical solution. For the first one, the slim tube test is widely accepted in the petroleum industry although its results may be tricky and lead to false conclusions in high degrees of physical dispersion. Moreover, it is time-consuming and expensive. For numerical and analytical solutions, a fluid phase behavior characterization is done by giving attention to numerical dispersion effects then a suitable EOS is assumed. Then an approach is adopted to calculate MMP, one dimensional compositional simulation is the most validated numerical approach as it is coherent slim tube results. Another valid approach is the multiple mixing cell method, it is highly similar to the compositional simulation in theory. In both approaches, the higher the number of cells or grid blocks, the lower the effect of numerical simulation, however, it is time-consuming. Otherwise, the analytical approach represents a powerful alternative to the numerical approach. As well, it is based on fluid characterization and EOS assumption. It can be applied to find the MMP of a system with an arbitrary number of components in the oil phase and injected gas. The global algorithm has made it faster in application than the numerical solution. The results of the analytical approach are well-validated and are in accordance with the numerical simulation and slim tube results. [35] [37]

The number of rigorous solutions increases with the number of fluid components. Yaun and Russell proposed the development of the analytical approach, which decreases the number of equations and unknown parameters, in addition to lowering the number of false solutions. [36]

Shokrollahi et al. reported a variety of empirical, analytical, and numerical solutions for defining the value of MMP in different conditions. [37]

One of the reported correlations was created by Yuan and Johns [38] in 2004. It is very relatively easier to apply because it does not need fluid phase characterization, and is more accurate than the other reported equations in Shokrollahi's work. Yuan and Johns have developed two correlations, the first one for pure CO₂ injection and the other one for impure CO₂ injection.

The one for pure CO₂ injection, which is of our interest, is validated within ranges of the temperature of 21.7 - 148.8 °C, MW of C₇₊ of 139 - 319, and PC_{2-C6} of 2% - 40.3%. Based on the results and the comparison they have reported, their correlations give much more precise results than most correlations developed before. They have linked MMP to reservoir temperature, C_{2-C5} components percentage, and molecular weight of C₇₊ present in reservoir oil, without the need for fluid phase characterization that was essential in analytical and numerical solutions. [38]

Yuan and Johns's correlation was chosen to find the MMP in this work. Its conditions and limitations suit the simulated case.

$$MMP_{pure} = a_1 + a_2 M_{C7+} + a_3 P_{C2-6} + T(a_4 + a_5 M_{C7+} + a_6 \frac{P_{C2-6}}{M_{C7+}}) + T^2(a_7 + a_8 M_{C7+} + a_9 M_{C7+}^2 + a_{10} P_{C2-6})$$

Equation 1- MMP correlation for pure CO₂ injection (from Yuan and Johns)

Where, M_{C7+} = molecular weight of C₇₊ components

P_{C2-6} = total molar percentage of C_{2-C6}

T = reservoir temperature

Coefficients, presented in table 1, were defined based on best fitting the correlation results for a number of cases using 9 oils, with the corresponding 41 slim tube MMPs results and 70 analytically calculated MMPs. The absolute average error in the 41 slim tube MMP values is 11.9% when analytical MMPs are the reference. MMPs from the correlation have an error of 6.6% compared to 70 analytical MMPs. [38]

Table 1- Best fit coefficients for pure CO₂ MMP correlation (from [38] Yuan and Johns 2004)

a_1	-1.4634×10^3
a_2	0.6612
a_3	-4.4979
a_4	0.2139
a_5	1.1667×10^{-1}
a_6	8.1661×10^3
a_7	-1.2258×10^{-1}
a_8	1.2883×10^{-3}
a_9	-4.0152×10^{-6}
a_{10}	-9.2577×10^{-4}

2.3 Diffusion and Dispersion

2.3.1 Diffusion in miscible fluids

In the oil industry, especially in EOR using miscible displacement (e.g. CO₂ injection), diffusion is a matter of interest because it is the mechanism that explains miscibility. Any two miscible fluids subjected to contact with one another slowly diffuse into each other with time until the initial sharp interface that separates them becomes a mixed zone. This mixed zone is a transition gradual zone from one pure fluid to another. Diffusion between miscible fluids is a result of the random motion of molecules with no need to apply a differential pressure or a gross flow motion. In this section, diffusion in absence of gross fluid movement will be discussed. [3]

If there is no gross fluid flow (change in volume), then the Molecular Diffusion Coefficient (D_o) between two fluids contacting one another at a cross-sectional area can be represented by Fick's equation. [3]

$$\frac{dG}{dt} = -D_o A \frac{\partial C}{\partial X}$$

Equation 2. Fick's diffusion equation

G = quantity of material diffusing across a plane

t =time (sec)

D_o = molecular diffusion coefficient (sq.cm/sec)

A = cross sectional area for diffusion (sq.cm)

C = concentration (vol %)

X = distance, cm.

However, when the displacement is in a porous medium, the cross-sectional area differs from the one in Fick's equation, therefore another coefficient should be introduced which is the *Apparent Diffusion Coefficient* (D). Therefore, in steady state diffusion, Fick's equation can be extended into: [3]

$$\frac{G}{t} = D \times \frac{\Delta C}{L}$$

Equation 3. Fick's extended equation

D = Apparent diffusion coefficient

L = length available for diffusion

This coefficient is dependent on the available average cross-sectional area and the total distance. D can be related to D_0 differently based on the model assumed to be representing the porous medium

1. **Straight Capillary model:** This model is highly criticized as a non-accurate representation of the porous medium. [3] For this model, $D/D_0 = 1$.

2. **Carman 45° model:** This model (Fig 23) shows that the average fluid movement in a porous rock should be directed about 45° to the net flow direction. Hence, if the net travelled distance is L, so the actual travelled distance is $\sqrt{2}L$. [3] By substituting this into Fick's equation, a new relation is found, $D/D_0 = \frac{1}{\sqrt{2}} = 0.707$.

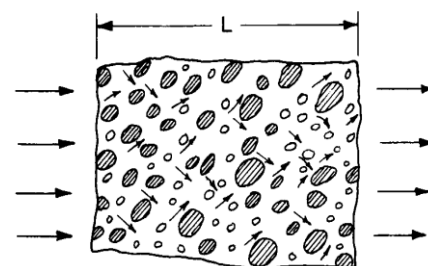


Figure 23- 45 degree flow model (from [2] Perkins and Johnston 1963)

3. **Real Porous medium:** Brigham, et al, and other investigators have noticed an analogy between electrical conductivity and diffusion. They reached a conclusion that the relation between the diffusion coefficient in a porous medium and the formation resistivity factor can be represented as: [2] [3]

$$\frac{D}{D_0} = \frac{1}{F\Phi}$$

Equation 4- Diffusion - Formation Resistivity Factor relation

F = Formation resistivity factor

Φ = Porosity

2.3.2 Dispersion in porous media

In the previous section we discussed diffusion in case of no gross fluid movement. However, mixing increases in the case of fluid flow. In a porous medium, the additional mixing is a result of uneven fluid flow or dispersion. Dispersion then can be referred to as the concentration gradient caused by fluid flow. If we are displacing a fluid by another miscible fluid in a porous medium, the volume injected vs. concentration measured at the outlet will yield an S-shaped concentration profile.

In porous media, two types of dispersion shall be considered. Dispersion in the same direction as gross fluid flow and dispersion transverse to the direction of gross fluid flow. These two types of dispersion are equal, so they should be considered separately. [3] Diffusion and

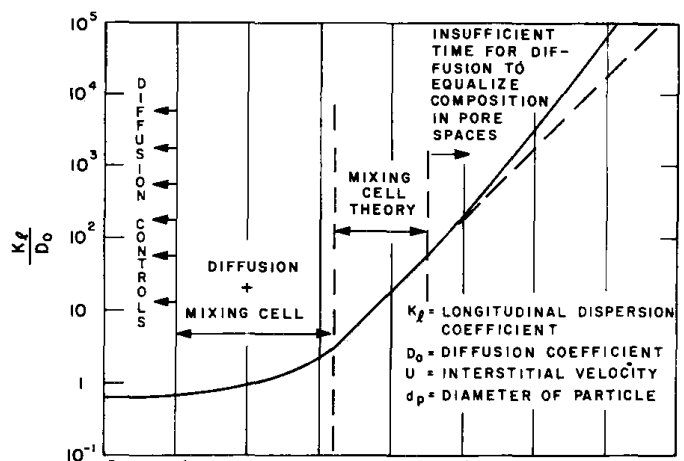


Figure 24-Range of validity of mechanisms of diffusion and dispersion in unconsolidated random packs of uniform size beads in laminar flow (from [2] Perkins and Johnston 1963)

dispersion are not explained by only one model, Fig. 24 shows different mechanisms that could be used with their range of validity.

2.3.2.1 Longitudinal dispersion

For studying the increase of fluid mixing in the longitudinal direction in a porous medium, investigators have considered dispersion in three geometries, capillary tube, a network of capillary tubes, and packs of granular material. [3] The latter will be discussed in the following lines.

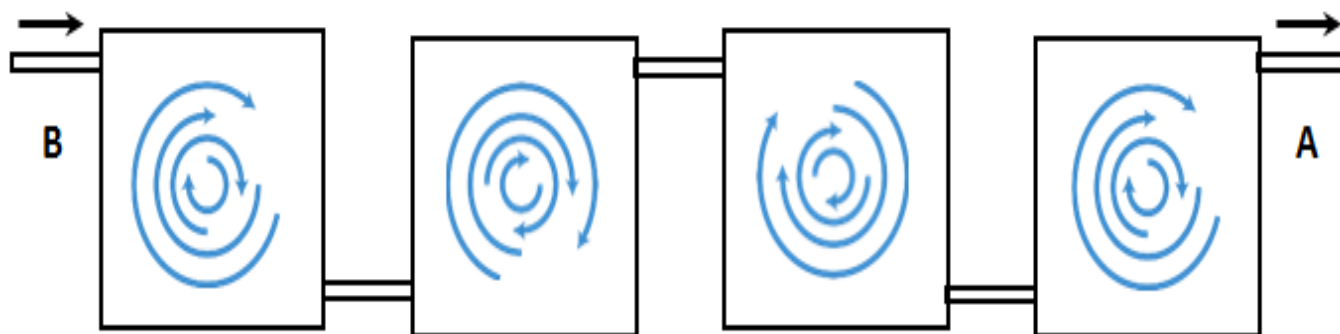


Figure 25- Porous medium being viewed as a series of mixing tank. (from permink.com)

Investigators have stated that the total longitudinal dispersion coefficient, K_L , is the sum of the *appurtenant (effective) diffusion coefficient* and *convective dispersion coefficient*, $K_L = D + E$.

To model a porous medium or a pack of granular material, the theory of *connected chambers* is applied. Aris and Amundson [7] investigated the dispersion in the connected chambers model. They used chambers or cells connected in series and uniform in size as shown in Fig 25. Chambers are initially filled with a fluid to be displaced then another fluid is injected at a constant rate from the inlet. The fluid composition in each cell is sustained uniform due to diffusion, grading from one pure fluid to another. Equation (Eq. 5) and a plot (Fig 26) that describe the model are reached by the previously mentioned investigators, considering Raimondi, et al, convective dispersion coefficient equation and showing values for his equation constants to represent random packs or porous media. [3] [5]

$$E = cU\sigma d_p$$

Equation 5- Raimondi, et al, equation

- $c = 0.5$ (constant)
- $\sigma = 3.5$ (a measure of increased dispersion due to heterogeneity)
- U = average velocity, cm/sec
- d_p = particle diameter, cm

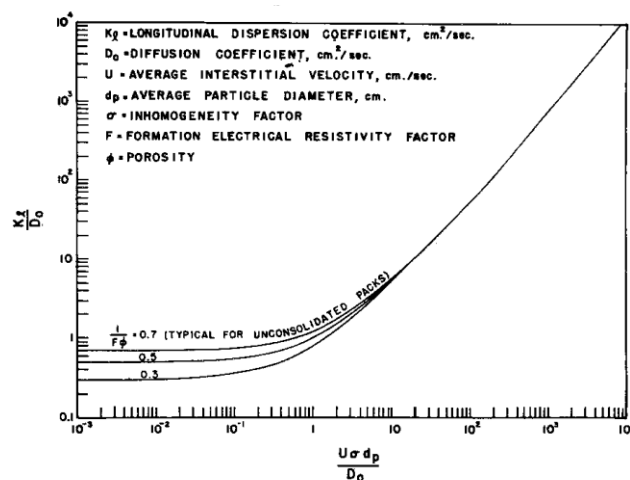


Figure 26- Longitudinal dispersion coefficients for porous media (from [2] Perkins and Johnston 1963)

$$\frac{K_L}{D_o} = \frac{1}{F\phi} + 0.5 \frac{U\sigma d_p}{D_o}; \text{ where } \frac{U\sigma d_p}{D_o} < 50$$

Equation 6- Total longitudinal dispersion equation

2.3.2.2 Transverse dispersion

If two miscible fluids are injected in this arrangement (Fig 27), where they should be separated at the entrance and only allowed to mix after they are injected into the porous medium. The development of the mixed area will increase in a direction perpendicular to the gross fluid movement. At the very beginning, the two fluids enter the porous medium as two separate streams. By advancing, a mixed zone starts to be created as a result of the diffusion of molecules between streams. Investigators call this mechanism, a “stream-splitting mechanism”. The typical S-shape of concentration is observed on any profile orthogonal to the gross fluid flow direction.

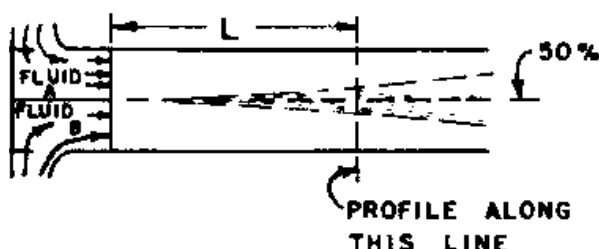


Figure 27- Transverse diffusion scheme (from [2] Perkins and Johnston 1963)

Investigators have described the transverse dispersion coefficient in several models by several equations.

Blackwell [8] described the transverse coefficient K_t in a porous medium with Eq 7 and Fig 28.

$$\frac{K_t}{D_o} = \frac{1}{F\phi} + 0.0157 \frac{U\sigma d_p}{D_o}; \text{ where } \frac{U\sigma d_p}{D_o} < 10^4$$

Equation 7-Total transverse dispersion equation

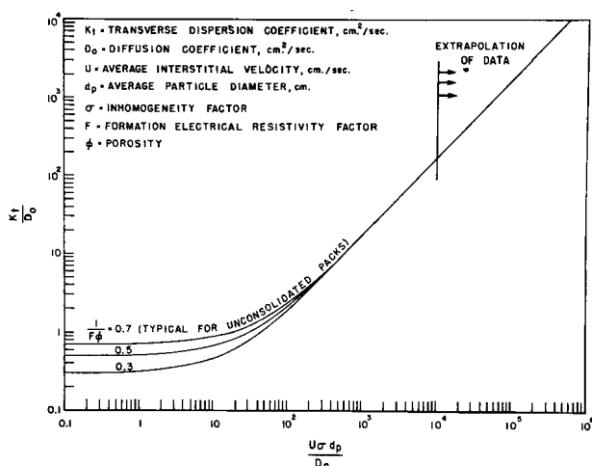


Figure 28- Transvers dispersion coefficients in porous media from [2] Perkins and Johnston 1963)

2.3.3 Factors affecting dispersion in porous media

- Porous media variables
 - Ratio of particle diameter to column diameter
 - Particle size distribution
 - Particle shape
 - Packing or permeability heterogeneities (as in natural rocks)
- Fluid variables
 - Fluids with different viscosities
 - Fluids with different densities
 - Fluids in turbulent flow
 - Effect of an immobile phase

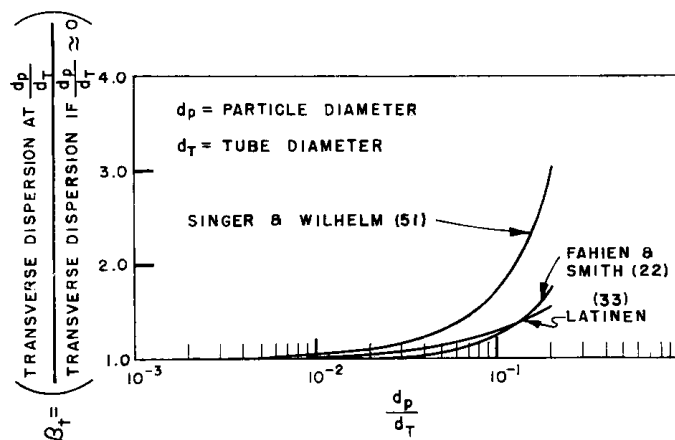


Figure 29- Effect of d_p/d_T on transverse dispersion in turbulent flow (from [2] Perkins and Johnston 1963)

2.3.3.1 Porous media variables

Ratio of particle diameter to column diameter

In laboratory experiments, spherical particles are packed into a cylinder to be used as a porous medium. High porosity zones, as large as two to three times particle diameters, exist near the cylinder walls. [4] This interruption to the regular packaging even extends to the entire area, it is not only exclusive to the vicinity of the cylinder walls. [9] This irregular packing will cause some sort of heterogeneity and it will surely affect both types of dispersion previously mentioned. [3] Perkins compared the results of three studies that studied the effect of cylinder walls on transverse dispersion in the case of turbulent flow (Fig 30). These studies concluded that the increase in transverse dispersion in the laminar zone is almost the same order of magnitude as in the turbulent zone.

$$\frac{K_L}{D_o} = \frac{1}{F\Phi} + 0.0157 \frac{U\sigma d_p \beta_t}{D_o}$$

Equation 8- Singer and Wilhelm correction for wall effect

β_t = factor to account for wall effect.

Particle size distribution

According to *Raimondi* and others, dispersion increases in a wide particle size distribution. In Fig. 30 Perkins reported the expected order of magnitude of dispersion vs. slope of particle size distribution. [3][5]

$$S = \log d_p|_{84} - \log d_p|_{16}$$

Equation 9- Particle size distribution slope equation

S = slope of the log-normal particle size distribution
 $d_p|_{84}$ = particle diameter of the 84% cumulative fraction
 $d_p|_{16}$ = particle diameter of the 16% cumulative fraction

Particle shape

Dispersion is generally higher in non-spherical packs than in spherical ones of almost the same volume. Fig. 31 shows a relation between the expected order of magnitude of dispersion and sphericity. This relation is quite representative of both types of dispersion in laminar flow. [3]

$$\Psi = \frac{A_s}{A_p}$$

Ψ = particle sphericity
 A_s = surface area of a sphere having the same volume as particle
 A_p = surface area of particle

Packing or permeability heterogeneities

Permeability heterogeneities may be found in:

- Random packs of spheres
- Cemented outcrops or reservoir rocks

The type of heterogeneities in cemented outcrops or reservoir rocks is the one that has our interest. The heterogeneities effect on dispersion is far more severe than expected from particle size. [3] *Perkins* reported the results of several studies done on sandstones and concluded an average value of 0.36 for $(d_p \sigma)$ as they are the controlling parameters of heterogeneity, to give correct values of dispersion coefficient in blocks of a few feet dimensions.

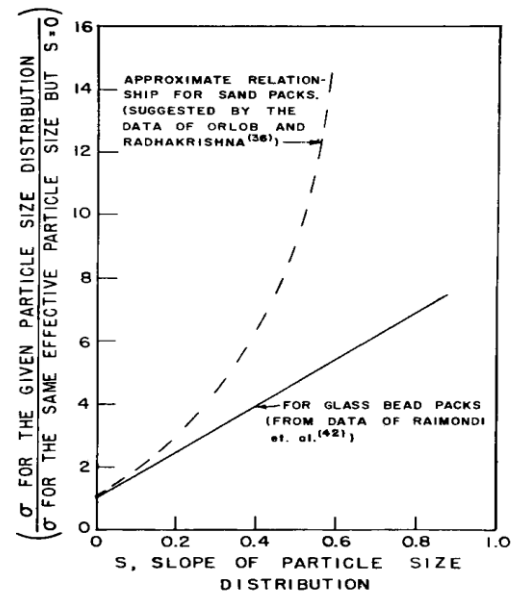


Figure 30- Effect of particle size distribution on dispersion (from [2] Perkins and Johnston 1963)

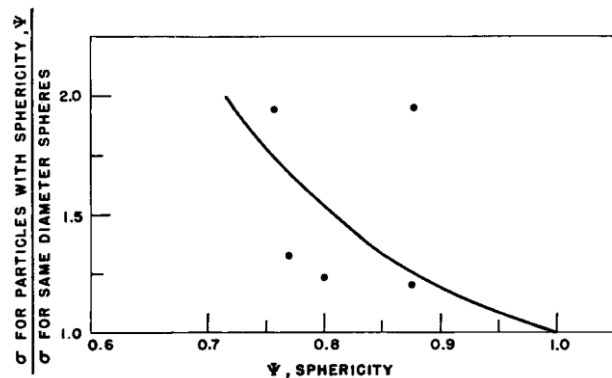


Figure 31- Approximate effect of particle shape on dispersion (from [2] Perkins and Johnston 1963)

2.3.3.2 Fluid variables

Fluids with different viscosity

Unfavourable fluids' viscosity ratio ($\mu_{\text{displaced}} > \mu_{\text{displacing}}$) will cause viscous fingers to happen. [3] An experiment was done by *Keable and Jones* on two miscible fluids flowing in a Hele-Shaw cell, where the less viscous fluid displaces the more viscose one. They changed fluids' viscosity several times creating multiple viscosity ratios, which is referred to as (M). Fig. 32 shows their results, it shows the higher viscosity fluid fingers evolution versus breakthrough time fractions at each viscosity ratio. At a low (unfavorable) viscosity ratio ($M=2$), fluid fingers are nearly not developed. While in higher ratios ($M = 5, 10, 20$) fluid fingers are developed severely. [11]

Generally, “ M ” refers to the mobility ratio which is a function of the viscosity ratio and relative permeability ratio. However, in this section “ M ” refers to the viscosity ratio.

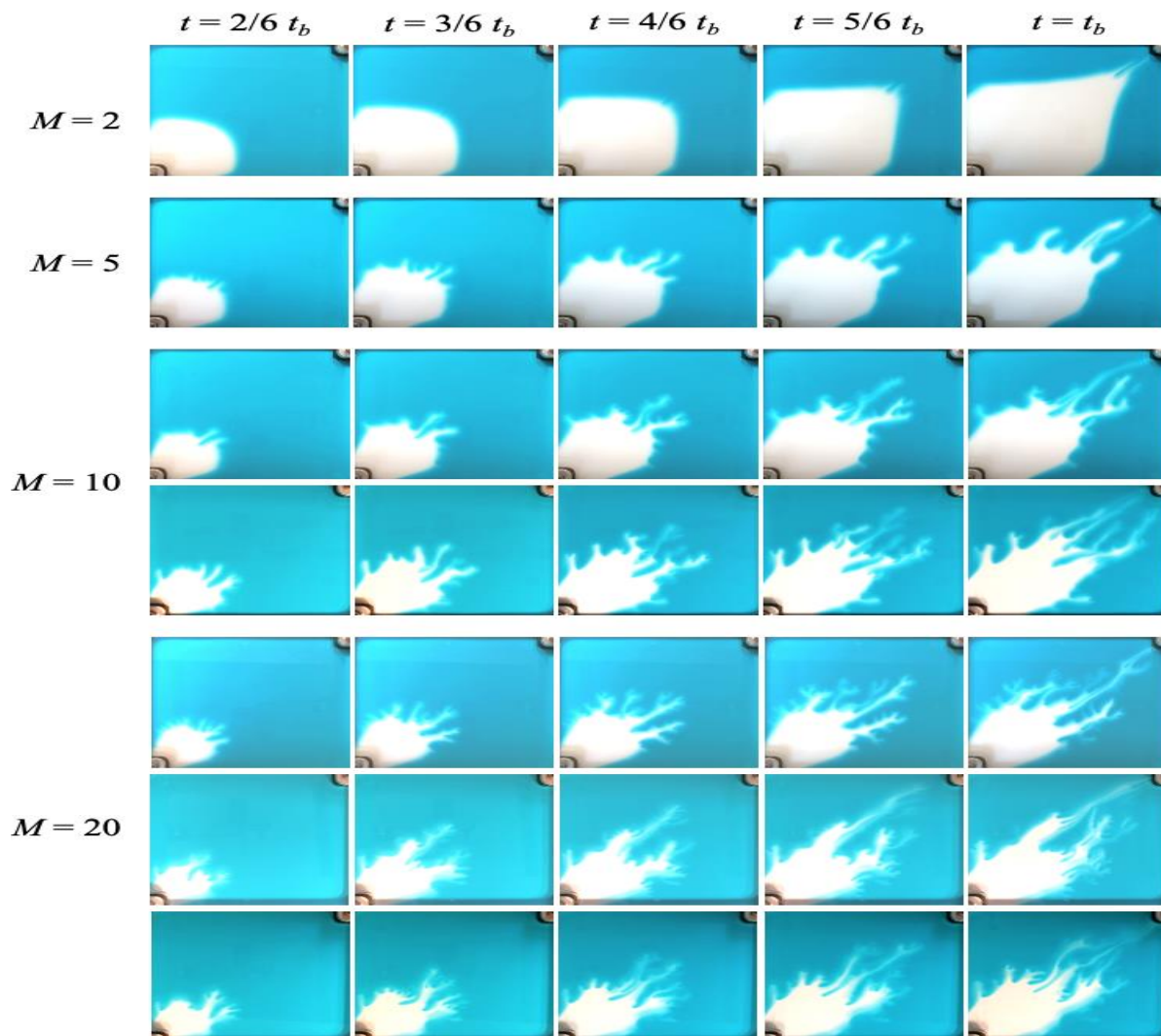


Figure 32- Evolution of miscible fingering patterns over time, t (expressed as fractions of breakthrough time, t_b) seen in experiments with different viscosity ratios (M), (from [11] Keable and Jones 2021)

Fingering is strongly related to unfavorable viscosity ratios, however, it is also related to permeability heterogeneities. [3]

A favorable viscosity ratio ($\mu_{\text{displaced}} < \mu_{\text{displacing}}$) limits the permeability heterogeneities effect, this means that fluid fingers will be minimized or not form at all. In this case, the mixing zone will be shorter and the dispersion coefficient will be definitely lower, it generally tends to straighten fluid interfaces within pores, until a limiting value of a favorable ratio. Fig. 33 shows one reported case that may give us a hint about the expected suppression order of magnitude. [3]

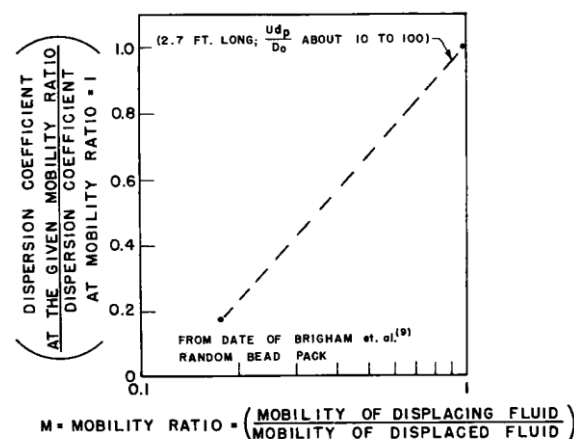


Figure 33- Suppression of dispersion resulting from favorable mobility ratios, (from [2] Perkins and Johnston 1963)

Fluids with different densities

In unfavorable gravity forces conditions, where a denser fluid is injected down dip so it will be above the less dense fluid, so-called “gravity fingers” are created, which promote random vertical dispersion. This randomness is due to permeability heterogeneities.

While favorable gravity forces will limit vertical (transverse) dispersion. The effect of permeability heterogeneities on dispersion, σ , which promotes unevenness of the front (gravity fingers), will be minimized by a factor that approaches σ . In addition, if the equalization of fluid composition by diffusion is not complete within each pore space, gravity will promote a further suppression in dispersion. It is an attempt to straighten the interface that leads to a piston-like displacement. [3]

Fluids in turbulent flow

Turbulence is not common in petroleum reservoirs, however, it may be encountered in laboratory experiments. In the study of turbulent flow, investigators express the dispersion coefficient in terms of “Peclet number” which accounts for particle diameter and fluid velocity beside the dispersion coefficient, to be properly correlated to the Reynolds number.

$$Pe = \frac{d_p U}{K}$$

Equation 10- Peclet number equation

For a fully developed turbulent flow, longitudinal Peclet number should approach a value of about 2.0 while transverse Peclet number should approach a value of about 11.

In a porous medium, there is a gradual transition from laminar flow to total turbulent flow, there is no sharp transition. A transition flow region is a region where both turbulent and laminar flow are present in different pores. Peclet numbers in this region can be described by the following equation. [3]

$$Pe|_{Re} = (1 - \nu)Pe_{\text{laminar}} + \nu Pe_{\text{turbulent}}$$

$Pe|_{Re}$ = average Peclet number at Reynolds number Re

ν = turbulence weighting factor (a value from 0 to 1, proportional to Re)

Effect of an immobile phase

Immobile gas phase has two major effects on liquid displacement and dispersion. For fluid displacement, it increases the liquid phase residual because when gas is present in small dispersed amounts, which cannot form a gas continuous phase, it isolates an amount of the liquid from the main continuous liquid stream. The average residual liquid saturation is about 2.5% and it may reach up to 5% with different set-ups. For liquid dispersion, the effect of the immobile gas phase depends on both the gas bubbles' location and on the porous volume structure; if the gas bubbles are trapped in the larger pores, this makes the smaller pores the effective ones for liquid flow. This results in less liquid dispersion because the heterogeneity effect (σ) decreases. The magnitude of this effect is influenced by the porous medium structure, the more uniform structure, the less the immobile gas influence.

2.4 Relative Permeability

Relative permeability can be defined as the ratio between the effective permeability to a definite fluid at a certain saturation and the absolute permeability which is defined at a 100% saturation. The used notations for oil, gas, and water are k_{ro} , k_{rg} , and k_{rw} , respectively. Relative permeability value changes with the fluid saturation as the corresponding effective permeability, while it is not a function of absolute permeability which is constant for a given medium. Its value ranges from 0, at saturations equal to below the critical saturation, to 1 at 100% saturation (monophasic flow). In two-phase or three-phase flow, the relative permeability of a given phase never reaches the value of 1, and the summation of the two or three relative permeabilities is always less than unity. [12]

In CO₂ injection, CO₂ has an effect on relative permeability values because on the one hand, the gas phase saturation is increasing, on the other hand, CO₂ changes the properties of the existing fluids. The altered relative permeability in turn has effects on pressure and recovery. [13]

Ghoodjani and Bolouri conducted an experiment to compare CO₂ and N₂ injection effects on rock and oil. They used sandstone cores saturated with light oil to the irreducible water saturation. They considered the N₂-oil relative permeability curve as a reference base because the effects of nitrogen on rock and oil are negligible. They reached a conclusion of which oil recovery and oil relative permeability in CO₂ injection are higher than in N₂ (Fig 34) injection due to the effects of swelling, viscosity reduction, and interfacial tension reduction (Table 2). In addition, GOR and gas production is higher in N₂ injection which includes an earlier breakthrough. The higher oil relative permeability in CO₂ injection results in lower differential pressure across the core, where there is further reduction due to CO₂ solubility. N₂ has negligible solubility, this makes gas phase compressibility promote a maximum limit for differential pressure. [13]

Table 2-Effect of CO₂ and N₂ on IFT, oil viscosity and swelling factor (from [13] Ghoodjani and Bolouri 2011)

	IFT (dyne/cm)	Oil viscosity (cp)	Swelling Factor
Initial	11.868	1.0509	1
N ₂	11.842	1.0503	1.0001
CO ₂	8.639	0.735	1.1022

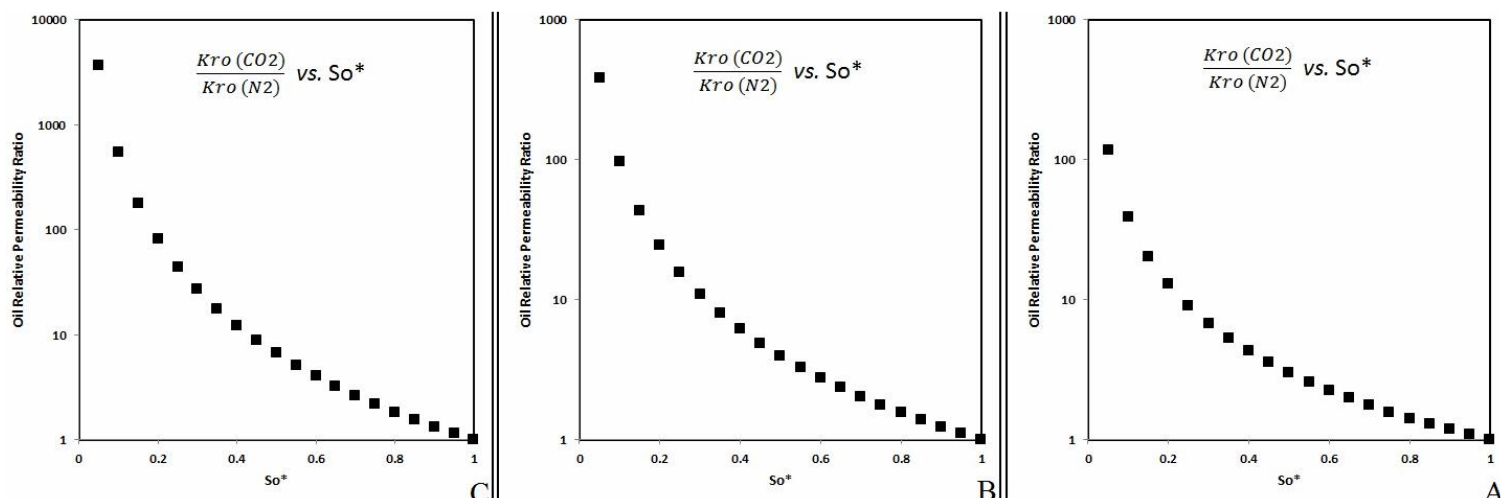


Figure 34- Ratio of oil relative permeability in CO₂ injection to N₂ injection (A) core C3 (B) core C1 (C) core S1. (from [13] Ghoojani and Bolouri 2011)

2.4.1 Oil Swelling (Expansion)

At the interface between CO₂ and oil, CO₂ gradually dissolves in oil increasing its volume. [13] The swelling factor can be measured by dividing the volume of oil with dissolved CO₂ by the volume of oil before dissolution. Simon and Graue developed a correlation between the swelling factor and CO₂ mole fraction limiting the volume measurement by the bubble-point pressure. The concluded correlation states that the swelling factor is a function of molecular size as well as the dissolved amount of CO₂ (Fig 35). [16]

As the swelling factor increases the residual oil saturation decreases, this results in a widening of the oil's relative permeability range and increases final recovery. [13]

The volume expansion due to swelling will create a drainage process that pushes oil to be produced from the production end, this is considered additional energy that is added in favor of oil phase movement. [15]

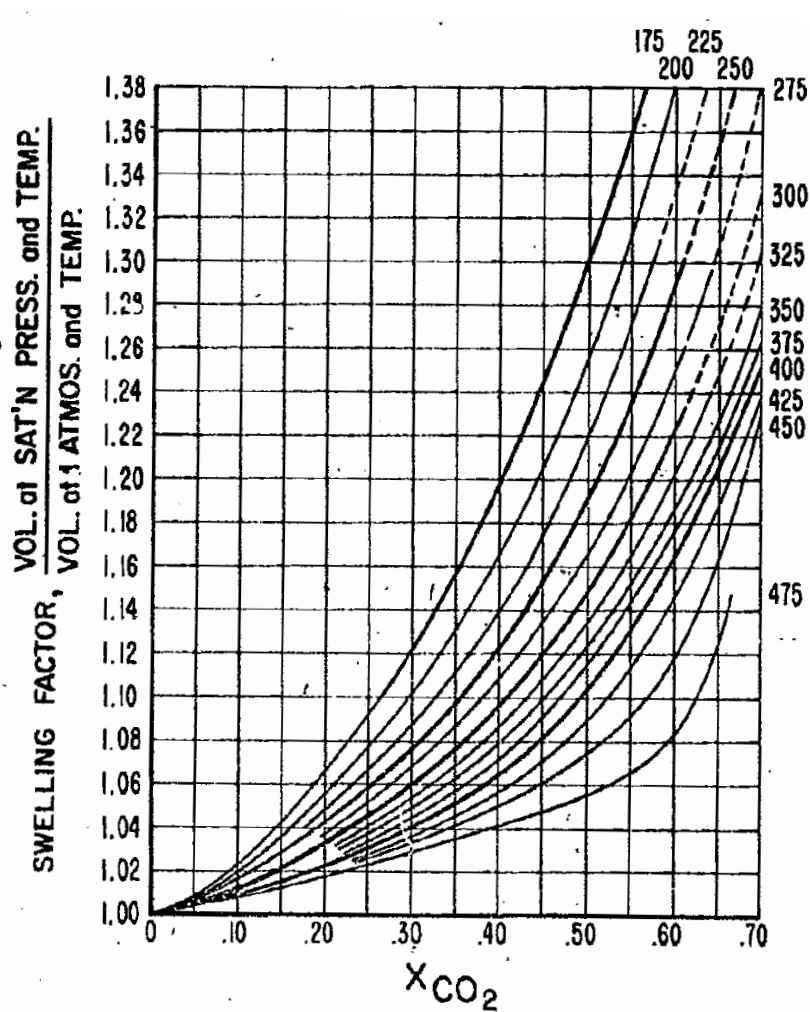


Figure 35- Swelling factor vs. CO₂ mole fraction (from [16] Simon and Graue 1965)

2.4.2 Interfacial Tension reduction

Dissolution of CO₂ into oil reduces the interfacial tension. [14] IFT has an important relation to fluid movement behavior, when it reduces, the energy consumed in the process of fluid movement is also reduced, and this affects the relative permeability curve. In theory, when IFT approaches zero, moving fluids act as a single fluid, which can be seen in the relative permeability curve as a straight line of unit slope. Therefore, it will be impossible to trap any of the fluids at the pore throat as a result of the relative permeabilities values that approach saturation values in each fluid. [13] In conclusion, oil relative permeability in CO₂ injection is more like a straight line than it is a curve [17] and it is more favorable to the movement of the oil phase than relative permeability in nitrogen injection (Fig 36). [13]

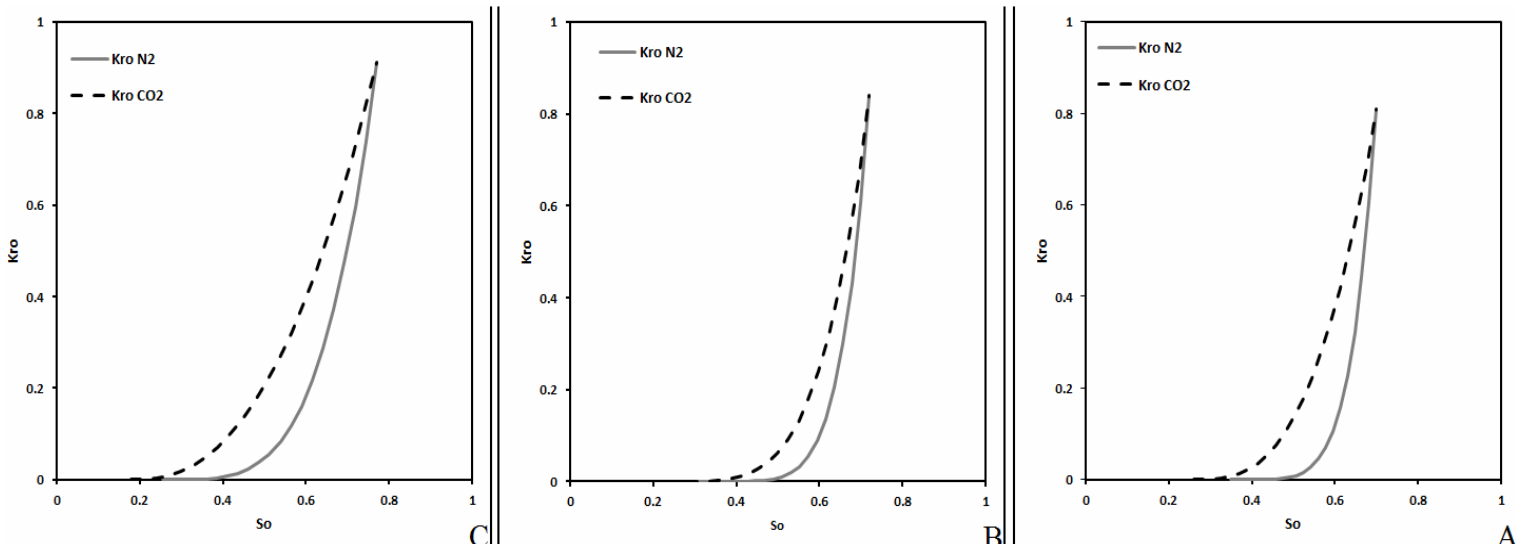


Figure 36- Oil relative permeability comparison in CO_2 and N_2 injection (A) core C3 (B) core C1 (C) core S1. (from [13] Ghoojani and Bolouri 2011)

2.4.3 Oil Viscosity Reduction

When CO_2 dissolves into oil, a significant reduction in oil viscosity occurs. The final value depends on the initial viscosity. For a high-viscosity oil, the reduction is higher than the reduction in the case of lighter oil. The viscosity reduction promotes an increase in the oil's relative permeability values and a decrease in the residual oil saturation. [13] However, it is noticed that viscosity reduction has no effect on the relative permeability ratio. [18] A correlation has been developed by Simon and Graue, based on experimental data of previous investigators, which relates the viscosity of a CO_2 -oil mixture (μ_m) to the original oil viscosity (μ_o) and to the saturation pressure at a constant temperature of 120 °F.

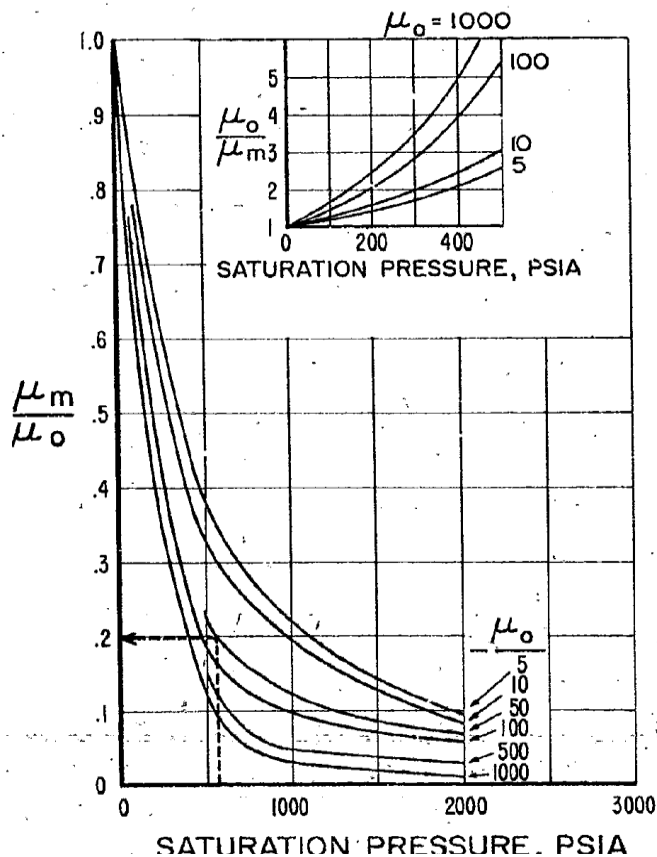


Figure 37- Viscosity of CO_2 -oil mixture at 120 F (from [16] Simon and Graue 1965)

2.4.4 Acid Effect on Rock

In CO₂ injection processes, a reaction between CO₂ and water takes place, resulting in carbonic acid. The rate of reaction is much faster in carbonate rocks than in sandstones. At high rates of CO₂ injection, porosity and permeability enhancement are recognized around the wellbore, as a result of calcite dissolution. In Ghoojani and Bolouri's experiment, this effect is not noticed due to the low rate of injection (0.3 cc/hour), so they did not account for relative permeability changes due to the acid effect. [13]



2.5 Capillary Pressure

Capillary pressure is the pressure difference between two connecting immiscible fluids due to a discontinuity in pressure across the interface between the two fluids.

There is a tendency for the curved surface between any two immiscible fluids to shrink into the smallest possible contact area. The degree of curvature defines the magnitude of the capillary forces, and it depends on the interfacial tension between rock and fluid (which is defined by wettability), the surface tension between the connecting fluids, pore geometry, and pore size. [12]

$$P_c = P_{\text{non-wetting}} - P_{\text{wetting}} = (2 \sigma \cos\theta) / r$$

Where, σ = surface tension between two fluids

θ = contact angle

r = capillary radius

In complete miscibility, there is no IFT between fluids, so they act like a single phase which means capillary pressure becomes zero. Usually, complete miscibility is assumed between CO₂ and oil in CO₂ miscible injection processes, however, this is not always entirely true.

Moodie and Ampomah conducted a quantitative analysis based on a simulation of CO₂ EOR in the Anadarko basin field. They accurately quantified the capillary pressure values vs. saturation for CO₂ and oil under reservoir conditions, then they ran the model by including the very small values of capillary pressure they obtained and they compared the results with the original model that neglected capillary pressure (assumed to be zero).

They found some significant differences between the two models, and concluded that complete miscibility between CO₂ and oil is not entirely developed. Simulations indicate that an amount of CO₂ is injected, which is enough to develop a supercritical CO₂ phase. Even at theoretical complete miscibility conditions, an interface should be present between the oil phase and CO₂ supercritical phase. [19]

2.6 CO₂ injection EOR process

In the US, oil and gas companies are very optimistic about the CO₂ flooding process because experience through the last decade has proven that it is a profitable EOR method. Another reason is that MMP could be reached in a wide range of oil reservoirs which makes them good candidates for the miscible CO₂ flooding application. [70]

Generally, an oil reservoir can be considered a good candidate for the miscible CO₂ injection EOR process if the oil gravity is above 25° API and at a depth of more than 915 m. Under these conditions, MMP is more likely to be reached hence miscibility between CO₂ and oil is achieved. [68]

Several investigators have put different criteria for the feasibility of applying miscible CO₂ flooding. Shaw and Bachu (2002) summarized these criteria that are mentioned in the literature until the year 2002 in table 3. [67]

Table 3- Criteria of applicability of miscible CO₂ EOR process (from [67] Shaw and Bachu 2016)

Reservoir Parameter	Geffen	Lewin et al.	NPC	McRee	lyoho	OTA	Carcoana	Taber & Martin	Taber et al.
Depth (ft.)		> 3.000	> 2,300	> 2,000	> 2,500	> 2.500	< 9,800	> 2,000	> 2,500
Temperature (°F)			< 250				< 195		
Original pressure (psia)	> 1.100	> 1,500					> 1200		
Permeability (mD)				> 5	> 10		> 1		
Oil gravity (°API)	> 30	> 30	> 27	> 35	30-45	>27	> 40	> 26	>22
Viscosity (cP)	< 3	< 12	< 10	<5	< 10	< 12	< 2	< 15	< 10
Fraction of oil remaining	> 0.25	> 0.25		> 0.25	> 0.25		> 0.30	> 0.30	> 0.20

In addition to the previously mentioned criteria, Bachu (2016) recommended other points to be taken into consideration. Before starting the CO₂ injection, the reservoir pressure has to be more than the MMP by at least 200 psi to reach miscibility. Reservoirs with low residual oil in place and a gas cap are not adequate for CO₂ flooding. Reservoirs with good pressure support due to a strong aquifer or a previous water-flooding process are good candidates for miscible CO₂ injection if the reservoir pressure is above MMP. Very heavy oil (< 15 °API) or very light oil (> 55 °API) shouldn't be considered for the application of CO₂ flooding because the resultant sweep efficiency will be very low. In terms of economics, small reservoirs are not recommended for this EOR process, instead, large reservoirs with a porosity between 0.11 and 0.33 are usually preferred. [71]

2.6.1 A case study from literature

This case was studied in details by [57] Tanner & Baxley (1992). The Wasson Denver unit is the world's largest EOR project in terms of the quantity of the injected CO₂ and the produced oil.

After a successful water flooding, the Sor was 40%. And a nearby natural source of CO₂ was discovered, then a CO₂ flooding project was initiated. Before CO₂ injection, a production period

started to reduce the reservoir pressure from 3200 psi to 2200 to increase the CO₂ volumetric efficiency. But at the same time, it is significantly higher than the MMP of 1300 psi.

Two zones in the field were devoted to two different processes, continuous CO₂ flooding, and WAG (WACO₂). This allows the comparison between the performances of the two methods.

In the continuous CO₂ region, the process design included the conversion of some wells that were previously used as water injectors into production wells. This conversion resulted in producing a large water bank at first, however, the process was eventually successful. An increase in oil production was noticed within days after the injection started. The results after four years of CO₂ injection show that oil production increased by 8000 bbl/d and WCT (water-cut) decreased from 86% to 69%. Soon after injection, the GOR value increased due to oil vaporization by CO₂. The advantage of this stripping phenomenon is that the CO₂ becomes enriched with hydrocarbons and this causes miscibility. However, its disadvantage appears in the wells where the gas (CO₂ + stripped HC) flow is dominant, in these wells hydrates can be formed in winter or cold nights.

The WAG zone, the oil production rate in the beginning was unsatisfactory, it was higher than the oil rate expected if water flooding continued, but in general, it kept declining. In addition, water injectivity was lower than expected, and this consumed more time to inject the planned water slug. Several problems were faced while attempting to make the injection rates comparable to the continuous CO₂ area, especially early cycles. The injectivity pressure was permitted above the fracture pressure only in water cycles. This led to a loss of 25% of injection fluid. This problem was eventually solved by changing the pattern from 9 spots into a line drive pattern increasing the number of injection wells from 33 to 60 wells. This process has managed to inject with the desired rate (cumulative rate) without exceeding the fracture pressure. For further improvement, the cycles were converted from six-month to yearly cycles to increase injectivity.

The comparison between the two strategies shows an advantage of the continuous CO₂ injection in terms of early EOR response, however, its CO₂ breakthrough was also early and gas production was very high in some wells that were later shut in. On the other hand, WAG has an advantage in terms of the final recovery. Besides, CO₂ production was very low over time, but there is a serious problem with injectivity and the oil production rate is declining over time without much of a significant difference from the water flooding response.

A new strategy was developed based on simulation optimization. The plan was to inject continuous CO₂ for 4 to 6 years then shift to 1:1 WAG. This strategy resulted in an early reservoir response due to continuous CO₂ injection, and a higher final recovery than the WAG process. Within a month of WAG injection using this strategy, CO₂ production rates began to drop, while oil and water production rates remained constant.

2.7 CO₂ injection process design

2.7.1 Food pattern

Tanner and Baxley studied the CO₂ EOR process performance in the Denver field. They have noticed a permeability preference in the east-west direction. By comparing production wells located east-west of the injection wells with the others that are located north-south, they found an earlier EOR response, earlier CO₂ breakthrough, and higher GOR in the east-west group. The north-south group showed a later EOR response, however, more sustainable for a longer period. [57]

In 2018, Kim et al. used machine learning techniques to define the best infilling wells locations in the Lost Hills field. The process they followed can be simply explained by that they assigned a

predetermined number of points (cluster) to be distributed randomly around each production well. Figure 38 shows all the random points that were added, where they were classified into Class 1 points (candidates to be a location for infilling wells) and Class 0 points (not candidates). This classification has been made based on the oil saturation, porosity, and reservoir thickness at each point. [58]

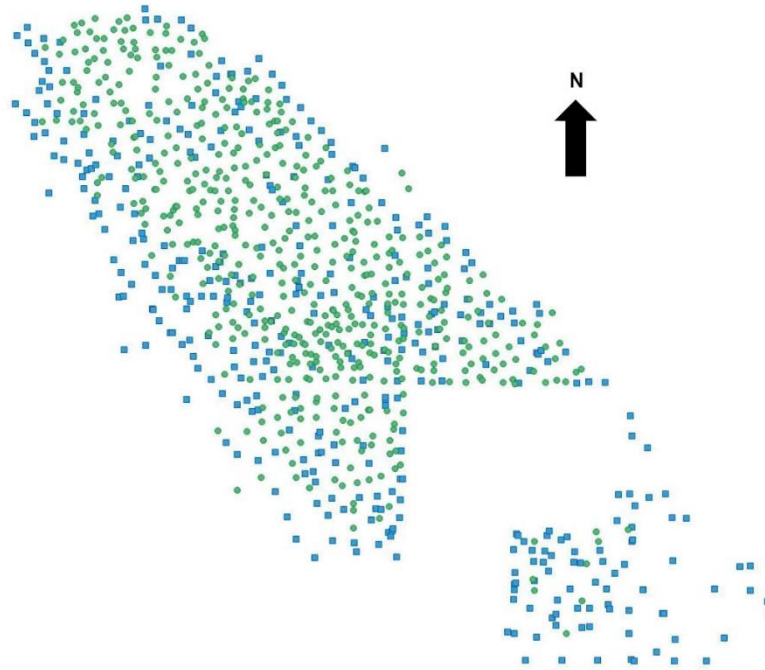


Figure 38- Possible locations for infilling wells, class 1 (green), class 0 (blue), (from [58] Kim et al. 2018)

After that the reservoir was divided into regions around each well and calculated their current oil in place COIP, however, the no-flow boundaries that are needed to define the regions in this field were not easy to be known, so they approximated the regions by the Voronoi diagram. This diagram is the creation of regions around each point, where lines are drawn to be at an equal distance from the closest two points (Fig 39), and finally, they reached the regions in fig 40.

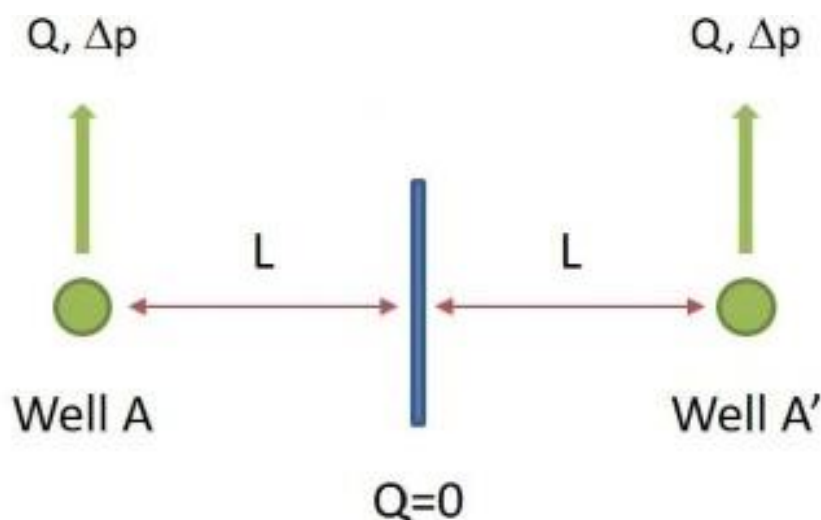


Figure 39- Concept of boundaries creation in Voronoi diagram (from [58] Kim et al. 2018)

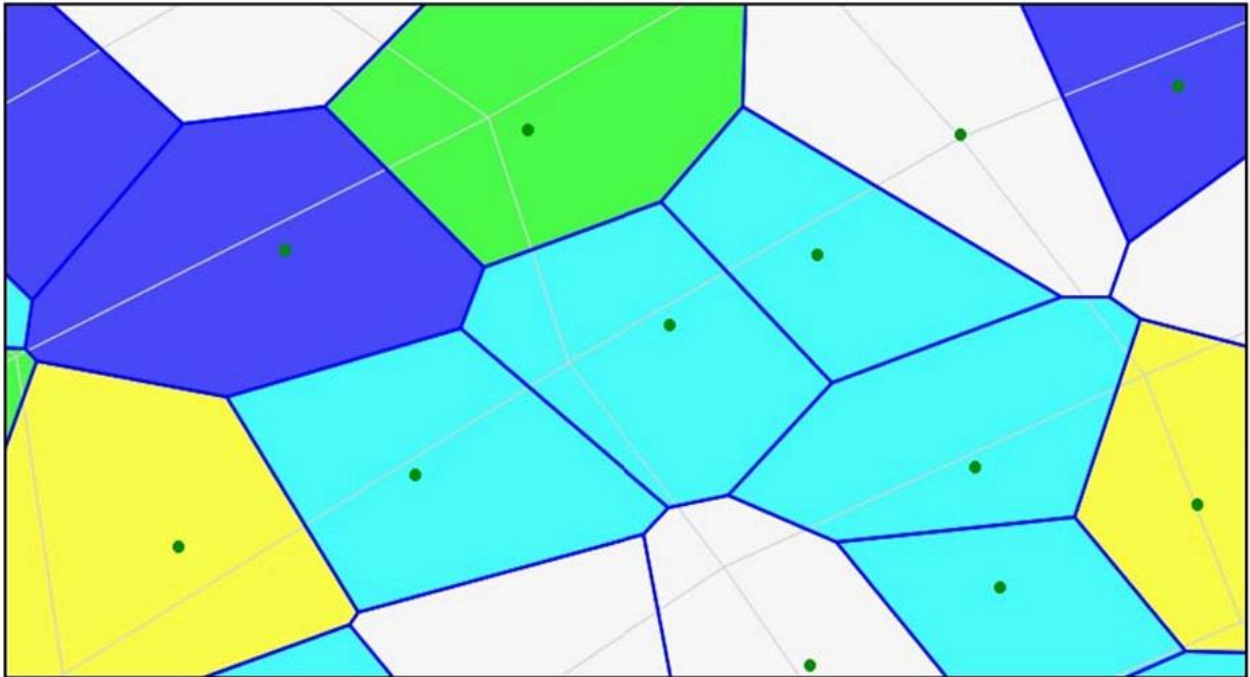


Figure 40- Reservoir divided into regions based on Voronoi diagram (from [58] Kim et al. 2018)

The well locations were then chosen by filtering out all points that are in the regions with low COIP/area. Then favoring the points that are close to the Voronoi boundaries, as long as they are far enough from any producers or injectors.

This machine-learning methodology has successfully recommended and ranked about 550 candidate locations in the Lost Hills field. [58]

In 2016, Perera and Gamage studied the effect of distance between injection wells on oil recovery. They found that the recovery decreases as the distance between the injection wells increases until about 1500 m the recovery starts to increase with the distance as shown in figure 41.

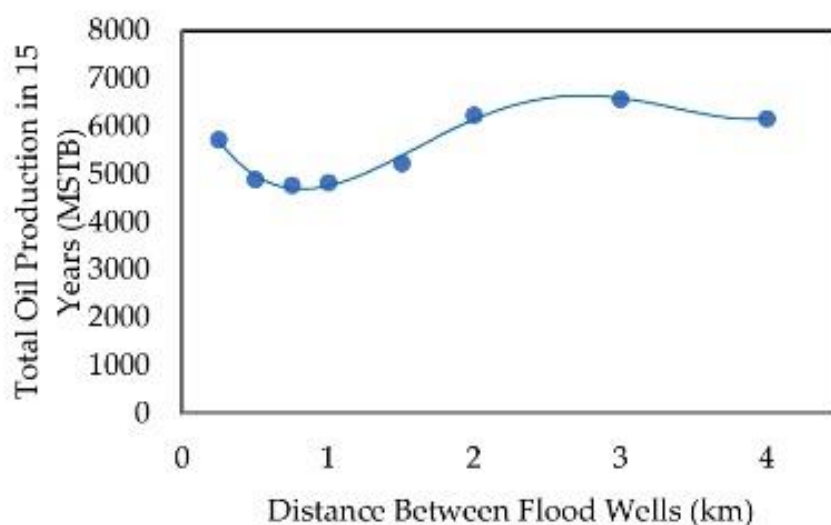


Figure 41- From [46] Perera and Gamage 2016

That's because when the distance increases, the area around a certain injection well that needs to be swept increases, so oil production from this area slows down. On the other hand, above the distance of 1500 m, the injectivity of CO₂ becomes higher because wells are sufficiently away from one another and the pore pressure created does not hinder the injection, this leads to higher oil production. Above 3000 m, there is no evidence of any relation between oil recovery and the distance between injection wells. [46]

In brief, the discussion covered the parameters that are related to flood patterns which are wells' locations, the orientation of producers relative to injectors, and the distance between wells, where each of them has its unique relationship with oil recovery that should be regarded.

2.7.2 CO₂ injection rates

Generally, oil recovery increases with the CO₂ injection rate. Perera and Gamage have observed that the relation between CO₂ injection rate and oil recovery is almost linear (Fig 42) in a sandstone reservoir in the Cooper basin. This response of the oil recovery is due to the increase in pressure that results from increasing the CO₂ volume that was injected in the specific period. Also, when the amount of the injected CO₂ is higher in a certain time frame, this results in an improvement in the recovery enhancement mechanisms, like swelling, viscosity reduction, and density reduction. [46]

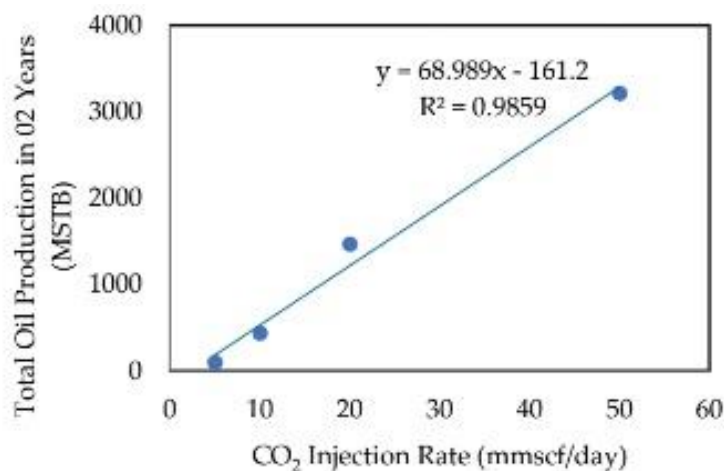


Figure 42- From [46] Perera and Gamage 2016

In 2020, Kaita and Ogolo reported a case in which the previous relationship was constrained by reservoir injectivity. They assigned an injection pressure of 5200 psi, and they ran 4 different simulations with 4 different CO₂ injection rates (500, 1000, 2000, and 3000 Mscf/day). The results show that the oil production rate increases with the CO₂ injection rate, however, beyond the 2000 Mscf/day there is no increase in oil production as shown in figure (43). By visualizing the actual CO₂ injection rate (Fig 44), it was noticed that it does not exceed 1500 Mscf/day. This means that the 5200 psi injection pressure does not support any injection rate above 1500 Mscf/day because of the formation injectivity. If the injection pressure is increased, the limit rate will also increase, however, it should not exceed the fracture pressure. Another effect that could be noticed is the early breakthrough in high injection rates. It can be observed in figure #, the time at which the production starts declining is the breakthrough time. This time becomes earlier when the injection rate is higher. However, the higher injection rates give higher oil production before the breakthrough time, the low injection rates can maintain higher oil production after the CO₂ breakthrough. [59] Therefore, the injection rate needs optimization.

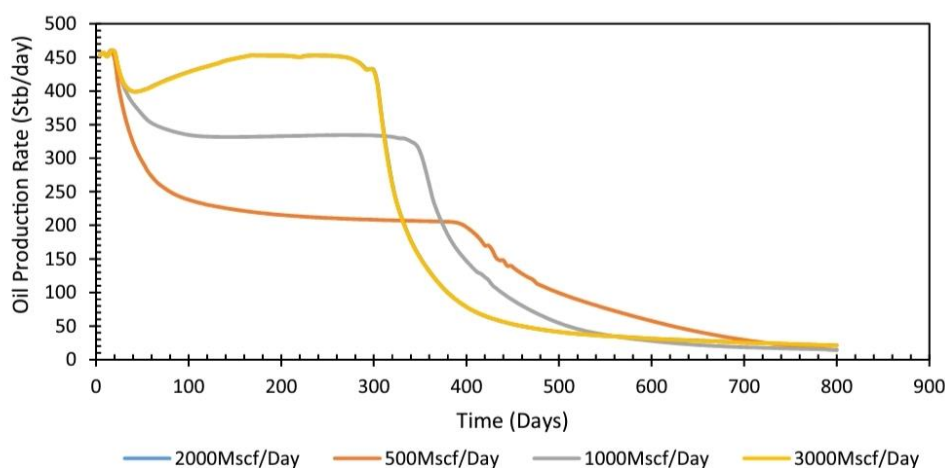


Figure 43- from [59] Kaita and Ogolo 2020

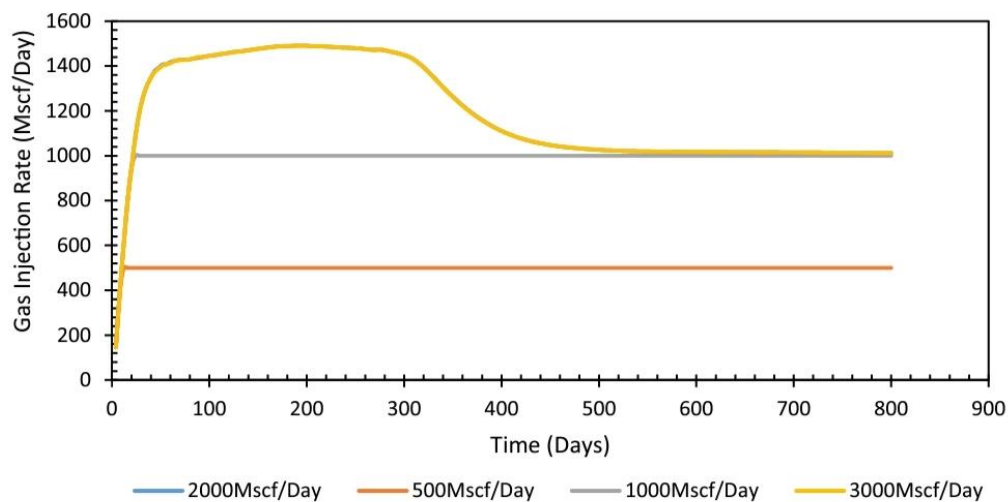


Figure 44- from [59] Kaita and Ogolo 2020

In 2012, Ghoodjani and Bolouri used the Green Balance simulator to predict the optimum CO₂ injection rate regarding the process economics. Figure 45 shows the relationship between the optimized CO₂ injection rate and the oil viscosity in two different degrees of reservoir heterogeneity. The optimum rate at each point was defined based on the same project expenses and oil price. The optimum CO₂ injection rate is higher with higher oil viscosity, however, beyond a certain limit, any increase in the injection rate typically increases recovery but it will not be enough to be economic.

The optimum rate is also affected by several parameters. It increases with the amount of OOIP. It also increases with oil prices because the added profit can cover more expenses in terms of CO₂ prices or injection system expenses. Moreover, the optimum injection rate is affected by the EOR plan duration. In short-term plans, maximum oil recovery is required so the optimum injection rate will be higher relative to long-term plans where high expenses of high injection rates should be avoided. [60]

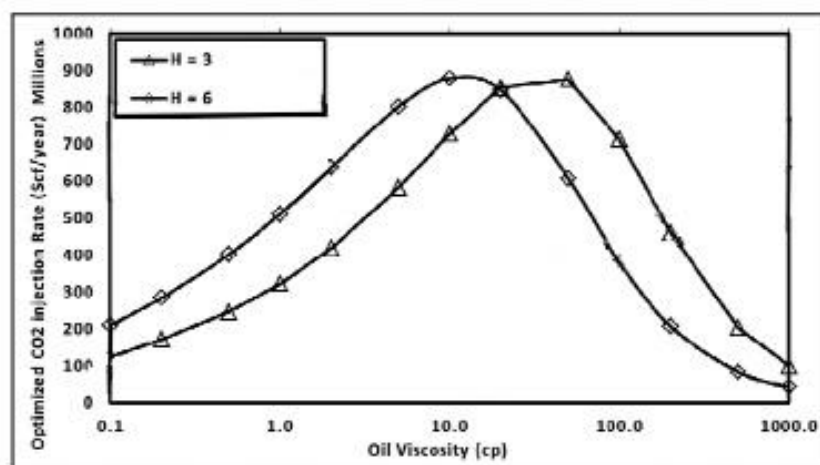


Figure 45- from [60] Ghoodjani and Bolouri 2012

2.7.3 Water injection rate

In 2016, Perera and Gamage reported an increase in the recovery factor with increasing water injection rate in CO₂-WAG injection as shown in figure 46. The recovery response was not as

powerful as the response due to increasing CO₂ injection rate. CO₂ has a greater impact on oil recovery due to its miscibility with oil, but water is not miscible with oil. [46]

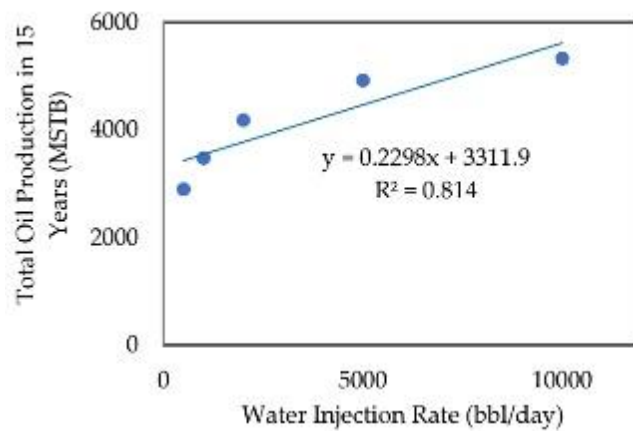


Figure 46- From [46] Perera and Gamage 2016

2.7.4 WAG Ratio

The WAG ratio is the volumetric ratio of the injected water to the injected CO₂ at the reservoir conditions. [64]

Ghedan (2009) summarized general guidelines for the CO₂-WAG ratio selection. [63]

- Continuous CO₂ injection: water injection is not applicable.
- Continuous CO₂ injection chased with water: preferred in reservoirs with a low degree of heterogeneity.
- Uniform CO₂-WAG: Used to reduce the CO₂ velocity, and improve vertical and areal sweep efficiencies.
- Tapered CO₂-WAG: Water cycles are usually longer in period and more in terms of injected volume than CO₂ cycles. It is used in case of a limited amount of CO₂ that is needed to suffice a certain recovery or duration.
- Gas chased CO₂-WAG: The WAG cycle is followed by a cheaper gas like CH₄, N₂, or air. It's used to reduce the cost or in the case of water-sensitive formations, therefore, water cycles should be minimized

Perera and Gamage reported in their previously mentioned case that in the miscible process, increasing the CO₂-WAG ratio results in a lower recovery (Fig 47); because the effect of CO₂ (miscible displacement) on oil recovery is higher than the effect of water injection (immiscible displacement). [46]

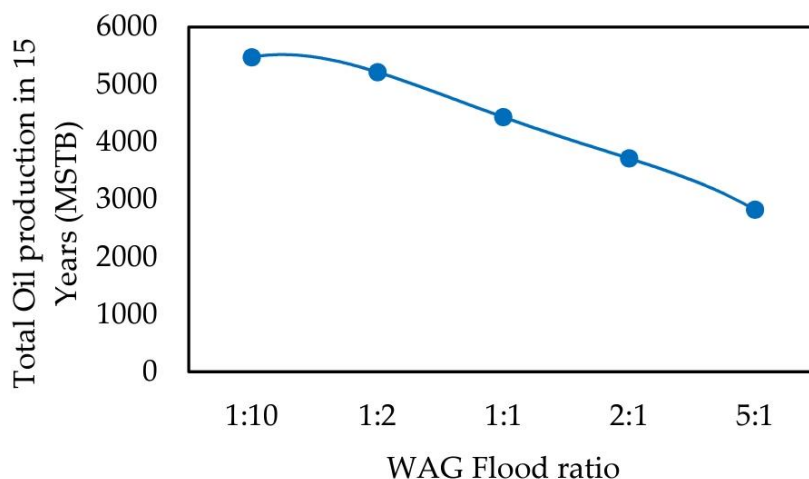


Figure 47-From [46] Perera and Gamage 2016

However, this inversely proportional relation is not general for all cases. The WAG processes in many cases give better oil recoveries than continuous CO₂ injection (which has a WAG ratio equal to 0), which means decreasing the WAG ratio does not necessarily result in better recovery.

For optimum oil recovery and production parameters, there is an optimum WAG ratio that differs from one case to another. This optimum value of the WAG ratio depends on the reservoir fluid and rock properties. [64] Ghahfarokhi and Pennell (2016) listed some factors that influence the selection of the optimum WAG ratio which are heterogeneity, anisotropy, wettability, reservoir fluid properties, miscibility condition, physical dispersion acidic reactions, relative permeability effects, IFT, and formation water salinity and pH.

For instance, the effect of wettability on the WAG ratio was studied by Huang and Holm in 1988. They worked on sandstone and chert core samples which were originally water-wet. These cores' wettability was then physically and chemically altered to get cores with different wettabilities, ranging from water-wet to strongly oil-wet. Cores were saturated with oil, then oil was displaced miscible by continuous CO₂ and CO₂-WAG to compare the efficiency of each process with different wettabilities. The comparison was done in terms of residual oil saturation after one pore volume (1 PV) of fluid injection. In the strongly oil-wet cores, Sor after the CO₂-WAG process was higher than that of continuous CO₂ with less than 5%. In mixed-wet cores, the difference was 15% to 20% in favor of continuous CO₂. In water-wet cores, the difference was more than 20% also in favor of continuous CO₂. [61]

Yang and Song (2015) ran numerical simulations and laboratory experiments to study the effect of the CO₂-WAG ratio on oil recovery and water injectivity in tight oil formations. They found that increasing the WAG ratio decreases water injectivity until a specific threshold further WAG ratio increase leads to injectivity improvement. In addition, the relationship between the WAG ratio and oil recovery is proportional until a certain limit of WAG ratio, above which oil recovery starts decreasing as seen in figure 48. [56]

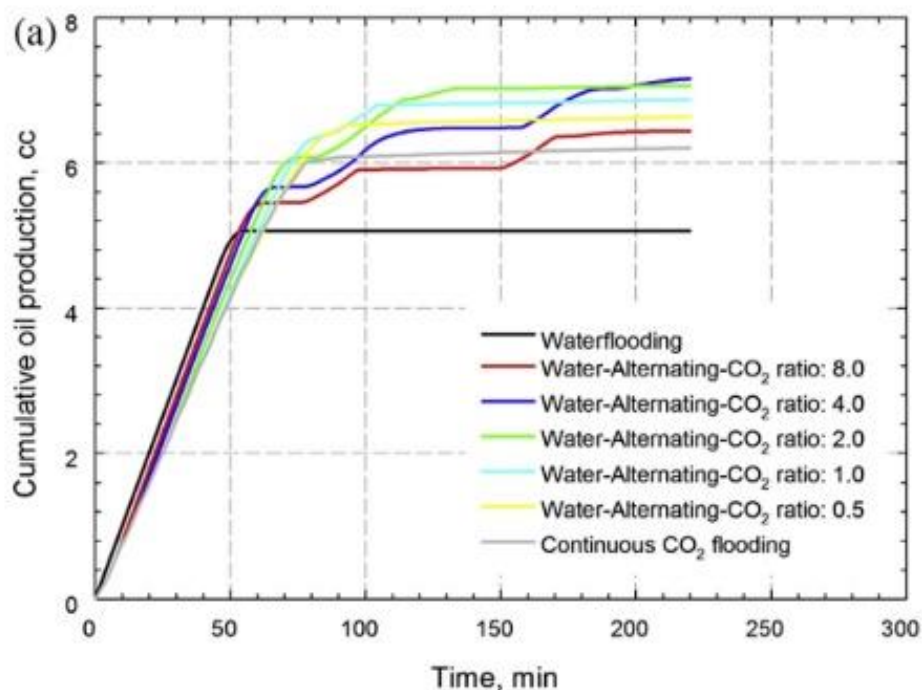


Figure 48- from [56] Yang and Song 2015

2.7.5 Total injected CO₂ volume

Saman and Curtis (2014) studied the history of the Devonian field, where a continuous miscible CO₂ injection process has been applied for years. They reported the relationship between the total injected volume of CO₂, in terms of hydrocarbon pore volume (HCPV), and the oil recovery factor (Fig 49). The oil recovery factor increases with increasing the cumulative injected volume. [65]

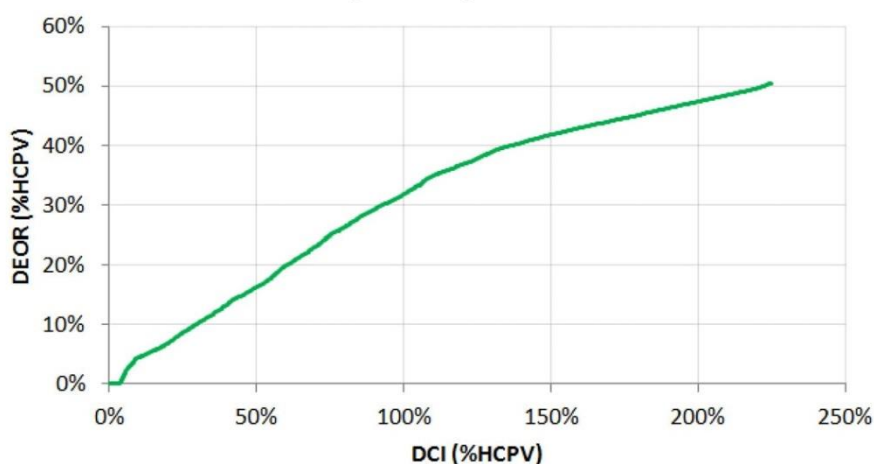


Figure 49- Oil recovery factor vs. total injected CO₂ in terms of HCPV (from [65] Saman and Curtis (2014))

Perera and Gamage (2016) reported in their previously mentioned case that oil recovery increases by increasing the cumulative amount of injected CO₂ until no more oil can be produced by further

injection. As shown in figure #, oil ceases to be produced above 5 HCPV of CO₂. [46] Therefore, in the case represented in figure #, the threshold above which there is no producible oil has not been reached yet.

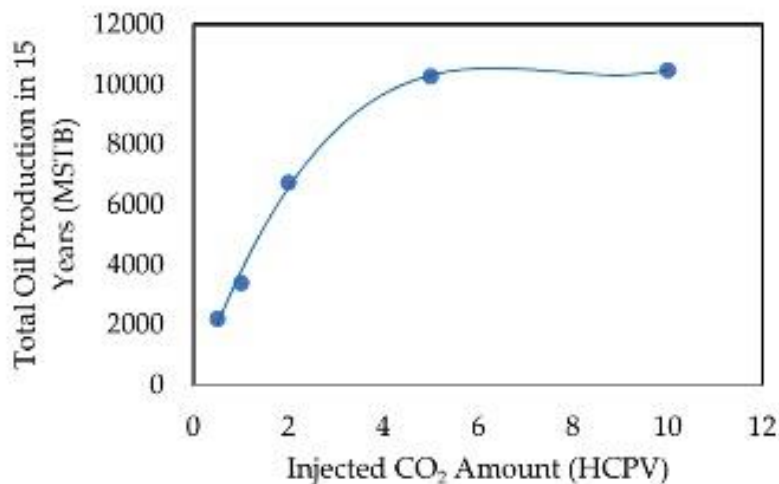


Figure 50- From [46] Perera and Gamage 2016

3 Numerical Simulation

Several simulation runs have been done. The Eclipse 300 simulation package by Schlumberger was used to generate the reservoir model, perform the simulations, edit, and visualize results.

The created reservoir model was used at all simulation runs without any changes in its properties. Two oil models were also used in all the simulation runs without changing their properties.

In this study, process design parameters are chosen to be objects of the performed sensitivity analysis so their values are modified in order to investigate their effect on the enhanced oil recovery of this process. These parameters are, flood pattern, CO₂ and water injection rates, WAG ratio, and total injected CO₂ volume.

In this section, the target of the numerical simulation, along with the previously mentioned models, their properties, and sensitivity analysis will be shown in detail.

3.1 Problem Statement

Based on the literature review that has been accomplished, a significant amount of oil can be additionally recovered by the injection of miscible CO₂. The additional recovery is a result of oil production enhancement mechanisms that occur simultaneously. These mechanisms are reservoir pressure increment, oil viscosity and density reduction, oil vaporization, and oil swelling.

The oil recovery may be improved even more by applying the CO₂-WAG process which improves sweep efficiency and minimizes gas fingering, however, the WAG ratio should be optimized to avoid backfire results.

In the stage of process design, factors like well pattern, CO₂ injection rate, water injection rate, WAG ratio, and total CO₂ injection volume are critical to obtaining a successful project.

In this study, the previously mentioned factors will be investigated to check the effect of each factor on oil recovery and production parameters, then the obtained results will be compared with past studies.

A numerical model was built, then a series of numerical simulations were run changing only one factor at a time to be able to conclude the relationship between the addressed factor and oil recovery

3.2 Reference Case

This case was simulated and its results were used as a reference for comparison with the other cases' results in the sensitivity analysis. In this section, the reference case will be defined in detail. Some parameters, in this case, were assigned after several simulations runs, e.g. well pattern and injection rates, as they have resulted in good values of enhanced oil recovery.

3.2.1 Reservoir model

The reservoir model used in this simulation project is built using FloGrid software, then exported as a GRDECL file. This file is imported to OFFICE software, to be converted to an INC file to be compatible with Eclipse 300 runs.

The following properties and conditions (Table 4) were adopted in the reference case:

Table 4 – Reservoir model data

Top	2950 m
Bottom	3000 m
Area	1000 m * 1000 m
Production drive	Depletion
Average reservoir pressure	300 bars
Reservoir temperature	90 °C
Porosity	0.24
Radial permeability	100 md
Vertical permeability	10 md
Initial water saturation	0.2
Irreducible water saturation	0.2

The reservoir model was assumed to be very deep (3000 m) to ensure that the pressure will be above MMP. It was also assumed that there is no nearby aquifer and that the production drive is a depletion drive, this will lead to a reservoir response that is only due to the injected fluid in the time period after the primary recovery.

3.2.2 Grid Selection

The reservoir block-centered grid model comprises of 6000 cells (20*30*10), with a vertical sealing fault at Y=15 (Fig 51). The x- and y-directions represent areal coordinates and the z-direction is vertical and increases downward. A box shape is assumed to represent reservoir geometry.

The reservoir is assumed to be homogeneous. A sealing fault separates the model into two hydraulically separated reservoirs. This fault speeds up the process of simulation, one side is assigned for continuous CO₂ injection while the other side is assigned for CO₂-WAG.

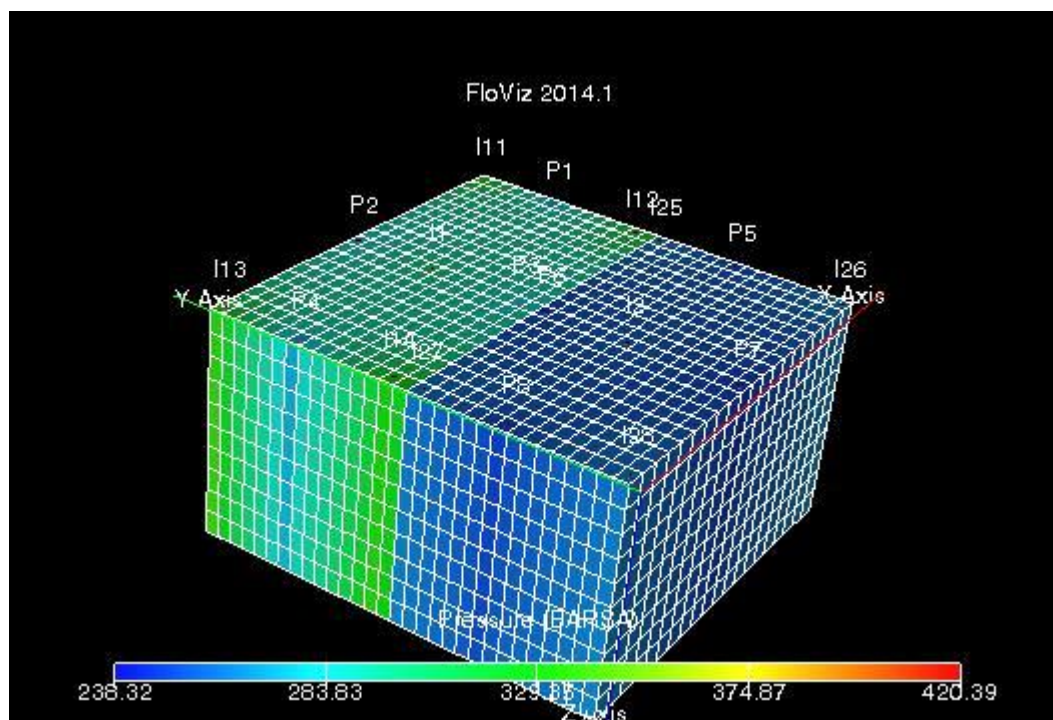


Figure 51- Grid model

3.2.3 Fluid models

Two fluid models were adopted in this simulation, the light oil composition is taken from Coats and Smart model [51], while the medium oil composition is assumed. PVO files for each model was generated using PVTi software, where intrinsic and PVT properties were defined in a file that is included in the Eclipse 300 data file.

Fluid components and fractions are as presented in table 5:

Table 5 - Fluids composition and fractions

Comp.	Light Oil	Medium Oil
N2	0.003	0.0
CO2	0.009	0.0005
C1	0.2847	0.1043
C2	0.1146	0.035
C3	0.0879	0.0283
C4	0.0456	0.0116
C5	0.0709	0.012
C6	0.1651	0.0257
C7+	0.2192	0.7826

After defining oil composition, simulations for flash, depletion, and constant composition expansion tests were run, as a result, the oil PVT properties are defined. Intrinsic and PVT properties that are needed in this study are tabulated in table 6.

Table 6 - Oil properties

Property	Light Oil	Medium Oil
Viscosity @ rc	0.2561 cp	0.9308 cp
Viscosity @ stc	0.7251 cp	1.1807 cp

Oil density @ rc	666.2 kg/m ³	888.8 kg/m ³
Oil density @ bp	619.7 kg/m ³	556.9 kg/m ³
Liquid density @ stc	792 kg/m ³	922.96 kg/m ³
Bubble point pressure	109.5 barsa	36.415 barsa
API oil gravity	46.63	25.35
Oil FVF @ rc	1.4983	1.0576
Oil FVF @ Psat	1.6109	1.0970
Gas FVF @ rc	0.0033	0.0034
MMP	184 barsa	212 barsa
Solubility, Rs	216.6 sm ³ /m ³	21.68 sm ³ /m ³
MW of oil @ rc	71.9257	158.7363
CO ₂ specific gravity	0.777	0.777
MW C7+	173	190
P C2-6	48.41 %	11.26 %

Results of the PVT tests simulations for the medium oil were not realistic, because the C7+ density was low. Therefore, heavier components were assumed to be present in C7+ which raises its molecular weight from 173 to 190. This assumption results in realistic results after running the test simulations. Stock tank oil properties like density, solubility, viscosity and etc., are taken from flash test results.

MMP is calculated from Yuan and Johns's pure CO₂ injection correlation [38]. This correlation was introduced in the literature review section. In brief, it links MMP to only the molecular weight of C7+, the total molar percentage of C2-C6, and reservoir temperature. The first two values are indicated in the previous table for both light and medium oil.

3.2.4 Equation of State

Peng-Robinson EoS was chosen to be used by the simulator software. Donald Robinson & Ding-Yu Peng developed their equation of state as an improvement on SRK EOS because the liquid volume prediction is overestimated compared to that obtained experientially.

$$p = \frac{RT}{v-b} - \frac{a}{v(v+b) + b(v-b)}$$

Where a and b are EoS model parameters, they can be calculated for pure components from the following equation.

$$a = \Omega_a \frac{R^2 T_c^2}{p_c} \alpha(T)$$

$$b = \Omega_b \frac{RT_c}{p_c}$$

$$\alpha(T) = [1 + m(\omega) \left(1 - \sqrt{\frac{T}{T_c}}\right)]^2$$

Where, $\Omega_a = 0.45724$

$\Omega_b = 0.07780$

The term b(v-b), enables this equation to be more accurate in liquid density prediction. The Zc value is taken as 0.307 which is more realistic than the value in SRK EoS, as it is closer to, for example, the Zc of C1. In addition, its prediction for Psat is more advanced than SRK in both pure hydrocarbon and non-hydrocarbon compounds. Lopez and Reif, have reported a detailed review of PR EoS development, general applications, and more than 200 modifications for pure compounds. [39]

3.2.5 Other data

Relative permeabilities and capillary pressure data were taken from Killough and Kossack (1987) [66]. The adopted data were rescaled by end-point scaling in the reference case data file.

Finally, fracturing pressure is calculated from the following formula (Eq. 11). The initial reservoir pressure (P_p) is 330 bars, the overburden pressure (P_{ov}) is taken as 678 bars, based on the assumption of an overburden pressure gradient of 1 psi/ft. The reservoir rock is assumed to be consolidated sandstone, this has led to an assumption of the matrix stress coefficient (K) to be equal to 0.75.), and this gives a fracture pressure of 591 bars.

$$P_{fr} = P_p + K(P_{ov} - P_p)$$

Equation 11- Fracture pressure equation

3.2.6 Injection strategy

Nine wells were used at each side of the fault. The following pattern was adopted (Fig 52), where “I” means injection well and “P” means production well. Other “well numbers” and patterns were simulated but the results of recovery were either very weak or takes more than 60 years to give the same recovery as the adopted one in 15 years. The distance between any two adjacent wells of the same group (production or injection) is about 700 m. The distance between any production well and the closest injection wells is 500 m. Both injection and production wells are open along the entire reservoir thickness, i.e. along all the 10 model layers

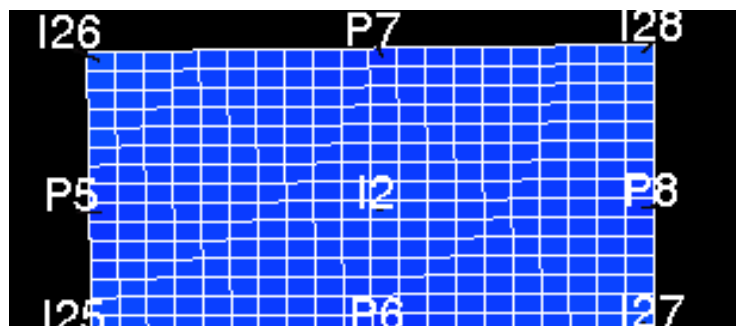


Figure 52- Well pattern in reference case

The water injection process was done for 3 years with injection rate 5000 m³/d per injection well prior to the initiation of the EOR processes to simulate the real field cases. Water injection was stopped at the mentioned time because the water cut started increasing rapidly.

After that continuous CO₂ and WAG injections started and were simulated for 20 years. The overall simulated time is 23 years.

The CO₂ injection rate was assumed as 300,000 Sm³/d, the water injection rate was assumed to be 5000 m³/d. Both fluids are injected with an injection pressure of 430 bars which is chosen to be below the fracture pressure of the reservoir rock. The chosen WAG ratio was 1 to 6. These values were reached after several simulations and they have given good results for the overall field recovery factor, water cut, and gas-oil ratio

Production wells' primary control parameter is oil rate, which was assumed as 1000 Sm³/d for each well. This value is conditioned by the minimum bottom-hole pressure, set equal to 240 bars with light oil production and 280 bars with medium oil production. If these values are reached production rate is forced to decrease until the pressure builds up to the determined limit.

The flowing bottom-hole pressure limit was chosen based on the density of the produced oil. For example light oil density equals 792 kg/m³ at standard conditions, a 3000 m column of this fluid will have a pressure of 230 bar at its bottom. So for oil to be produced from the bottom to the surface the flowing bottom hole pressure needs to be more than 230 bar plus the pressure losses in the well. Then assuming a threshold Pwf of 240 bar is enough to achieve this purpose.

The following flow chart in figure 53 summarizes the applied processes, production and injection rates, and control parameters.

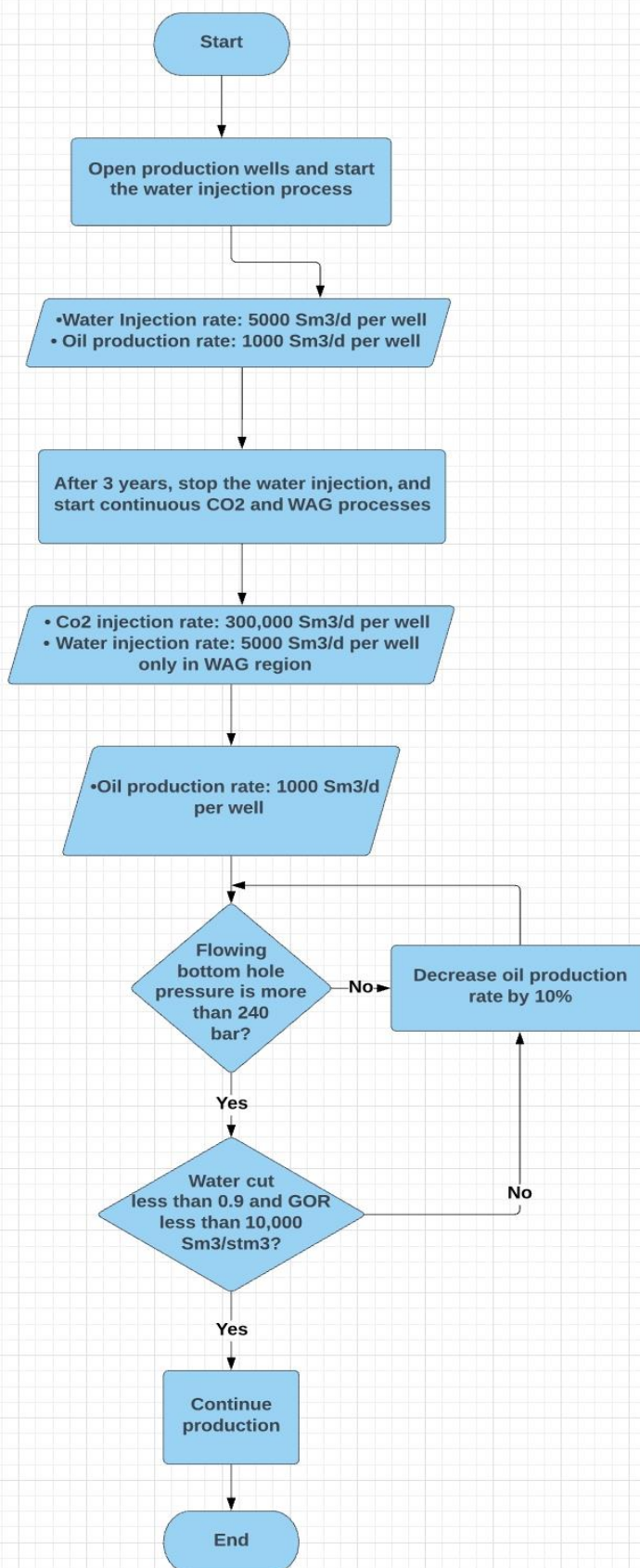


Figure 53- Flow chart of the process strategy

3.3 Reference case results

Light oil results

The recovery factors are presented in (Fig 40). The blue curve represents the results for the region with continuous CO₂ injection, while the green one represents the results for the region where WAG was applied. The overall recovery factor values are very high because this is an assumed model with no heterogeneities. The recovery in the first three years is due to the water flooding process, and it is around 0.3.

Throughout the entire EOR simulation time, average reservoir pressure was maintained to be higher than both MMP and bubble point pressure as indicated in the injection strategy.

WAG injection strategy results in recovery higher than that achieved with continuous CO₂ (Fig 54), the difference between the two recovery factors after 10 years is about 0.15 in favor of the WAG injection. After the three years of water injection, WAG injection resulted in an additional oil recovery of 0.57 while continuous CO₂ injection added an additional recovery of 0.42. Ideally, if both injection processes continue for an infinite time, all the oil in place will be recovered; because CO₂ is miscible with oil and capillary pressure is assumed to be zero, this means CO₂ will not trap any oil.

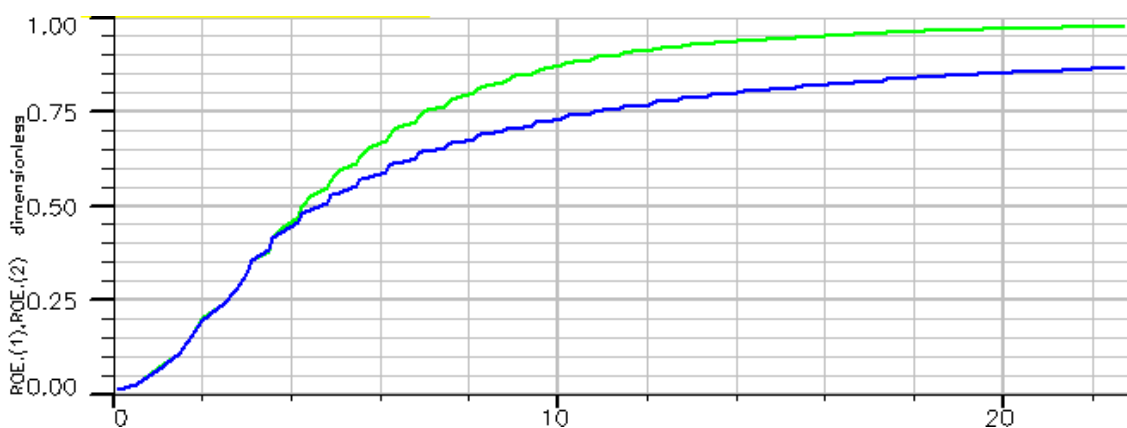


Figure 54- Recovery facot after 23 years simulation time, WAG region (green), CO₂ region (blue) (LGT_OIL)

The field water cut after 10 years of production is about 0.75 (Fig 55). Nearly all the produced water comes from the WAG region after the three years of water injection have ended as shown in Fig 56. While the gas-oil ratio (Fig 57) after 10 years has reached 2000 Sm³/STm³, this value increases dramatically in the following years due to the injection of CO₂ gas.

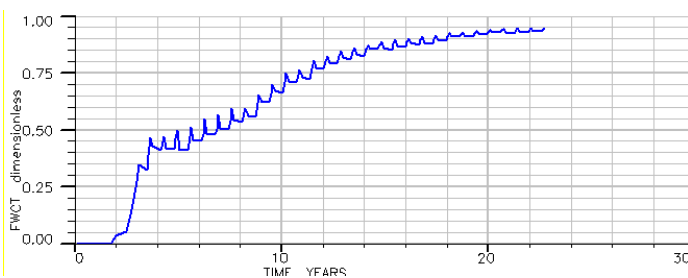


Figure 55- Reference case field water cut (LGT_OIL)

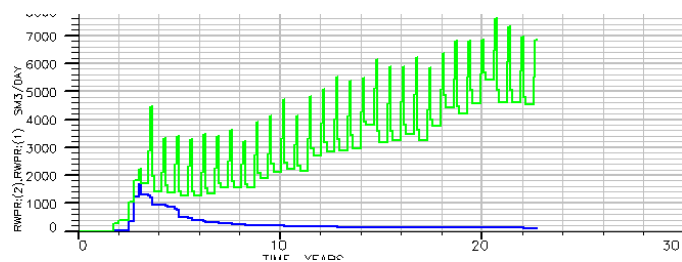


Figure 56- Reference case water production, WAG region (green), and CO₂ region (blue) (LGT_OIL)

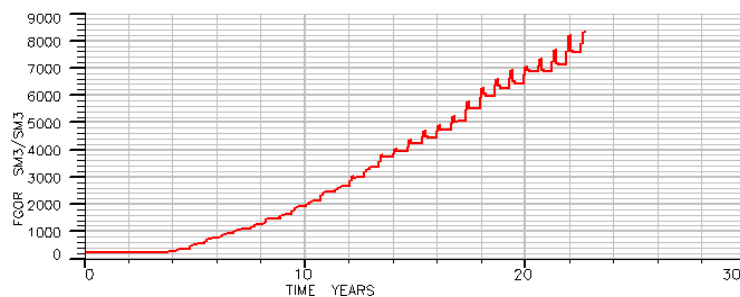


Figure 57- Reference case field GOR (LGT_OIL)

Medium oil results

The recoveries of medium oil in both WAG and continuous CO₂ injection regions were lower than that with the light oil. The recovery factor of the WAG region after 20 years was around 0.83, with an increment (after the three years of water injection) in the recovery of about 0.56, after the three years of the water flooding process. While in the continuous CO₂ region, the values of total recovery after 20 years and increment in recovery are 0.58 and 0.31 respectively (Fig 58).

For instance, in continuous CO₂ region, it took the medium oil model 20 years to reach an oil recovery factor of 0.58, on the other hand it took the light oil about 7 years to reach the same value. This indicates that the light oil is much faster in recovery than medium oil.

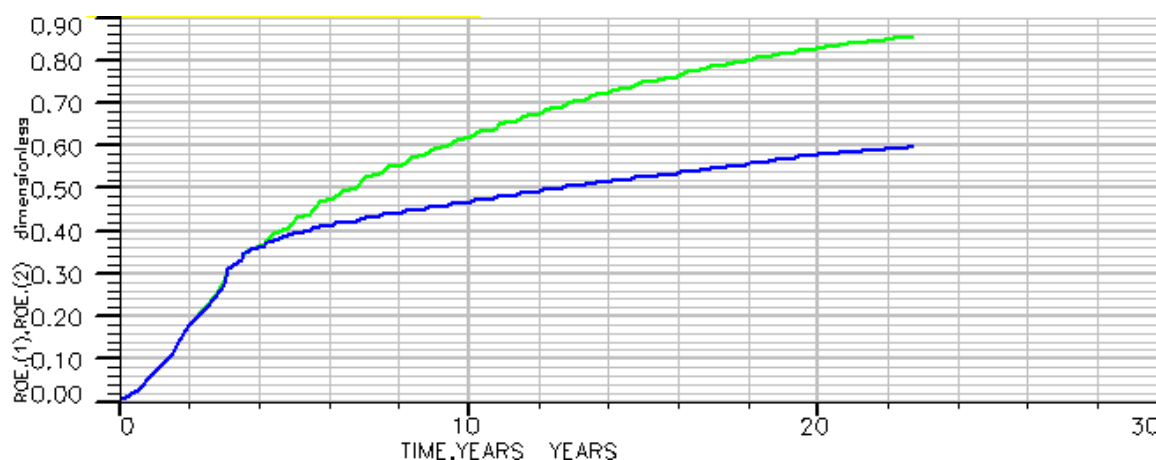


Figure 58- Reference filed recovery factors, WAG region (green), CO₂ region (blue), (medium oil)

The field water cut after 10 years of production is about 0.6 (Fig 59). Most of the produced water comes from the WAG region after the three years of water injection have ended as shown in (Fig 60). The gas-oil ratio after 20 years has reached 2000 Sm³/STm³ (Fig 61), which is the same value reached in light oil after only 10 years.

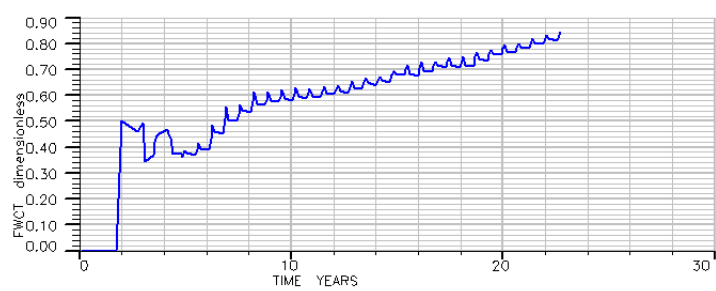


Figure 59- Reference field water cut (medium oil)

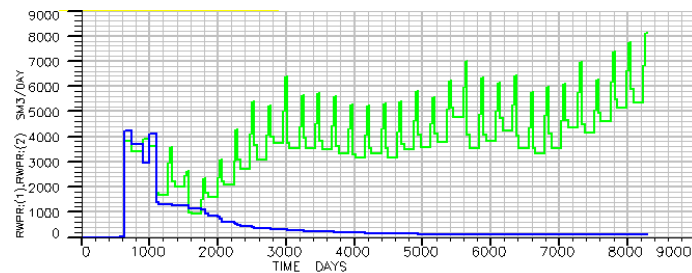


Figure 60- Reference field water production, WAG region (green), CO2 region (blue), (medium oil)

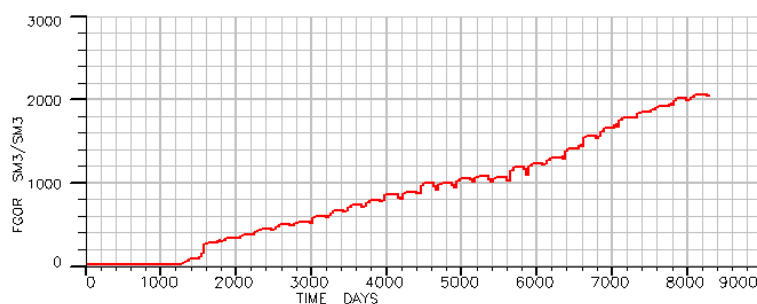


Figure 61- Reference field GOR (medium oil)

3.4 Sensitivity analysis

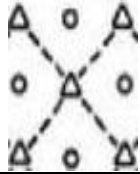
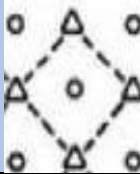
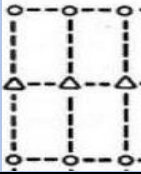
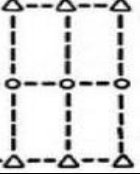
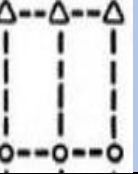
All numerical simulations are performed with two simultaneous runs, one for continuous CO₂ injection and the other one for WAG injection. To make this possible and to make the data results representative of each case, the reservoir model is separated by a sealing fault into two hydraulically separated pools. The fault transmissibility is zero and a very high threshold differential pressure is imposed on the fault face in both directions to ensure that there will not be any flow between the two pools. In addition, all simulation runs are done two times, once for light oil and once for medium oil.

The strategy of the sensitivity analysis is made up to serve the purpose of the study. First, a base case was built and run. The results of this case are to be considered as a reference for all the subsequent simulation runs. Some parameters are selected to be changed, in order to study their effect on enhanced oil recovery by comparison with the reference case recovery.

To study the effect of a certain factor, only that factor is changed from the reference case, then one or more simulations are run to see the effect on enhanced oil recovery. The study of each factor is done once at a time so that the model response is solely due to the change in only this factor.

Table 6 shows the factors considered in this study and their values. Each one of the cells in blue represents a new value of the investigated factor different from the reference case, which means every single blue cell represents two separate simulation runs, one for light oil and one for medium oil. Therefore, this separate simulation run targets the effect of a certain factor or parameter to be investigated.

Table 7- Sensitivity analysis strategy

Investigated factor	Reference case Simulation	Value in Sim 1	Value in Sim 2	Value in Sim 3	Value in Sim 4
Flood pattern	Regular five-spot 	Inverted five-spot 	Line drive 1 	Line drive 2 	Line drive 3 
CO2 injection rate (sm3/d) per well	300,000	100,000	200,000	400,000	500,000
Water injection rate (m3/d) per well	5000	1000	3000	4000	6000
WAG ratio (water/gas)	1 : 6	1 : 10	3 : 1		
Total CO2 injected volume in HCPV @ 10 years	1.3 HCPV	0.6 HCPV	0.95 HCPV	1.65 HCPV	2 HCPV






3.5 Results and Discussion

3.5.1 The effect of flood pattern

The well patterns were changed 4 times with respect to the base case, as indicated in the sensitivity analysis strategy table. Four separate simulations were run then the results were compared with the base case and with one another. The recovery factor results for five simulations of light oil are presented in Fig 62 and Fig 63. Generally, for all the simulations, whether with light or medium oil, the recovery from the region where WAG was applied is higher and faster than the recovery from the region where continuous CO2 was applied, regardless of the used pattern. In addition, light oil recovery is higher and faster than medium oil in all correspondent simulations. However, the pattern case comparisons in both of them are nearly the same, so presenting only light oil results will be sufficient.

Oil recovery with line drive pattern (3) compared to the others is much lower. The only different parameter that distinguishes this case from all the other cases is the distance between production and injection wells, which is about two times the other cases. In the other cases this distance is at least 500 m while in the line drive pattern, this distance is 1000 m at least. This result is consistent with Perera and Gamage's [46] results on the same topic. They reported a case in which oil production decreases as the distance between wells increases until 1500 m after that the relation is reversed and production increase with distance. The reason for that if the distance increases this means the area appointed for a certain injection well to sweep increases, therefore oil recovery from this region slows down. On contrary, the relation is reversed after the distance of 1500 m above which injectivity of CO2 is higher because wells are sufficiently away from one another and the pore pressure created does not hinder the injection.

Table 8- Key legend of the well patern simulation figures

5-Spot pattern (reference case)	
Inverted 5-spot pattern	
Line drive 1	
Line drive 2	
Line drive 3	

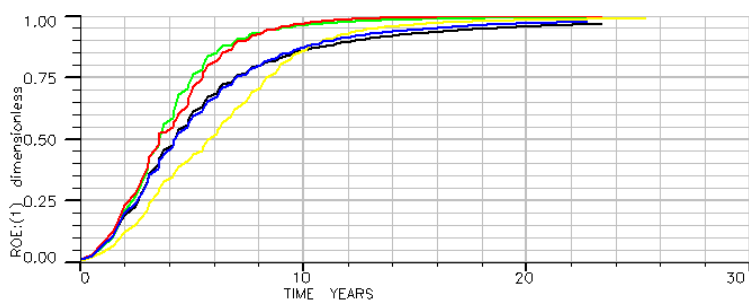


Figure 632- WAG region recovery factors (light oil)

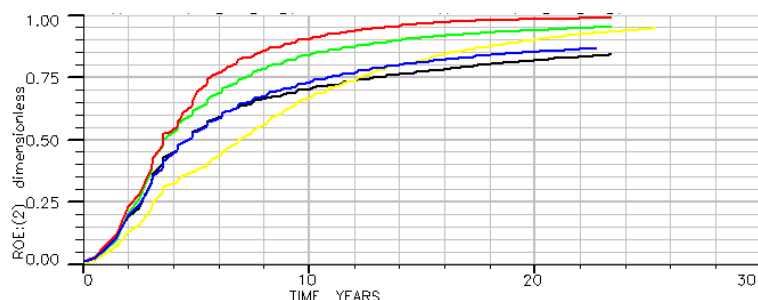


Figure 623- Continuous CO2 region recovery factors (light oil)

Line drive 1 and Line drive 2 have the best results in terms of recovery, however, line drive pattern 1 has an advantage in terms of economics, because the rates and total amounts of injected fluids are lower. This is evidenced by comparing their results of total injected CO₂ (Fig 64) and GOR (Fig 65).

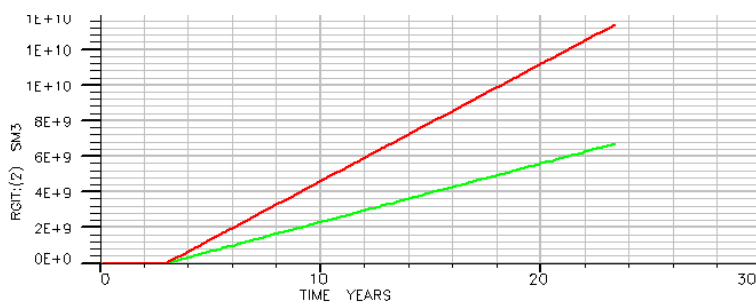


Figure 64 -CO2 total injected volume in continuous CO2 region

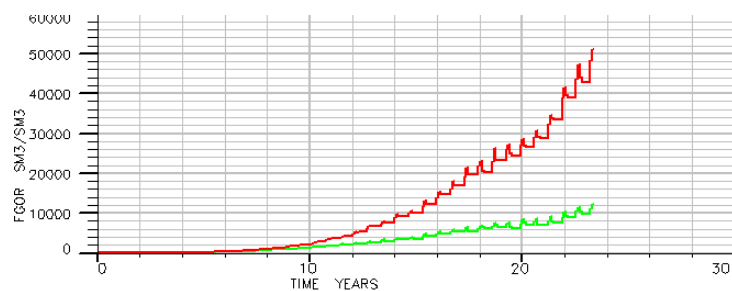


Figure 645- GOR in continuous CO2 region

In brief, the final recoveries after 20 years in the WAG region are comparable, while the difference in the continuous CO₂ region is at most 0.15. If early recovery and production parameters are considered, flood patterns, including good numbers and well spacing, will be of great importance in both WAG injection and continuous CO₂ injection processes.

3.5.2 Effect of CO₂ injection rate

Four simulations have been run and compared to the reference case to study this effect. Values of the CO₂ injection rate were changed as indicated in the sensitivity analysis strategy (table 6). The found results show higher oil recovery with a higher CO₂ injection rate. This conclusion is general for all the cases, WAG or continuous CO₂, and light or medium oil. Field recovery for different CO₂ injection rates with light oil is shown in Fig 66. The difference in the incremental recovery after 10 years between injection rates of 500,000 Sm³/d and 100,000 Sm³/d was about 15%. An important observation that should be reported, is the high disparity amongst cases in terms of the resulting gas-oil ratio. As shown in Fig 67, the GOR is increasing with increasing injection rates. These results are consistent with Perera and Gamage's [46] results on the same topic. The proposed explanation for their results was as follows, the more the amount of injected CO₂ in a certain time period, the more

pressure is added to the system, which resulted from the increase of the amount of CO₂ molecules that get in more voids and contact with more oil in a specific time period.

Increasing CO₂ injection rates is generally beneficial for oil recovery, however, it is limited to two critical factors. The first is economics, in the high injection rate cases, GOR is also high, which results in a higher total amount of CO₂ to be injected and higher costs for injection facilities.

The second limitation is the fracture strength of the cap rock. A higher injection rate in a short period could result in a dramatic increase in the pore pressure around the injection well and damage the cap rock. This severe problem may result in CO₂ injection losses or even migrating back into the atmosphere.

Table 9- Key legend for the effect of CO₂ inj. rate figures

300,000 Sm ³ /d (Reference case)	Blue
100,000 Sm ³ /d	Green
500,000 Sm ³ /d	Red

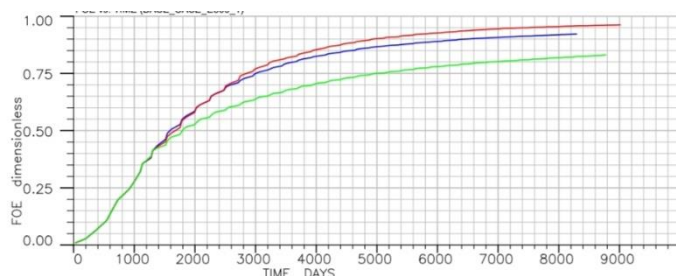


Figure 666- Field recovery factors for different CO₂ injection rates (light oil)

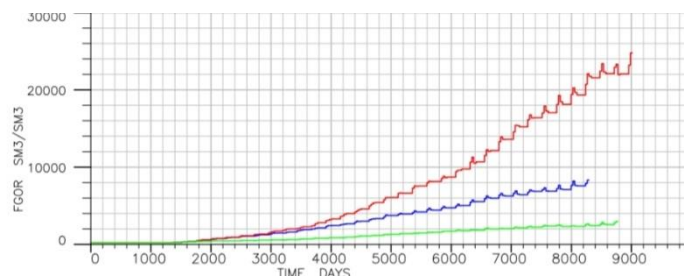


Figure 657- Field GOR for different CO₂ injection rates (light oil)

3.5.3 Effect of water injection rate

To study this effect, 4 separate simulations were run and compared with the reference case. The results indicate that there is an increase in the final oil recovery with increasing water injection rate in the WAG area in both light and medium oils, however, the recovery increment is not as high as in the case of increasing CO₂ injection rate. This is logical because the dominant displacement process is miscible displacement and CO₂ is the reason for this kind of displacement.

Aside from that, there is an interesting result that may help in the optimization of this section of the process. As shown in (Fig 68), the water injection rate in the first three years of water injection is not following what was intended to be in cases of 6000 m³/d and 5000 m³/d water injection due to low water injectivity into the formation. This problem has disappeared in the WAG period for the 5000 m³/d injection rate, however, it continues for nearly all of the WAG injection period for the 6000 m³/d. While the 1000 m³/d case has been injected normally as planned.

A possible explanation for these observation could be that the applied injection pressure (430 bars) only supports injection rates that are below a certain value. In the first three years of water injection, 5000 m³/d and 6000 m³/d injection rates are higher than the threshold value. However, the threshold injection rate is improved after the injection of CO₂. The relation between the WAG ratio and water injectivity was also studied by Yang and Song [56], they proved that injection of CO₂ slugs enhances water injectivity into the formation.

As observed from the results, in the water injection process, water injectivity into the formation becomes harder as the injection rate increases. In WAG injection, the limit for injection rate rises to a higher value than in the water injection process.

Table 10- Key legend for water injection rates

5000 Sm ³ /d	Blue
6000 Sm ³ /d	Red
1000 Sm ³ /d	Green

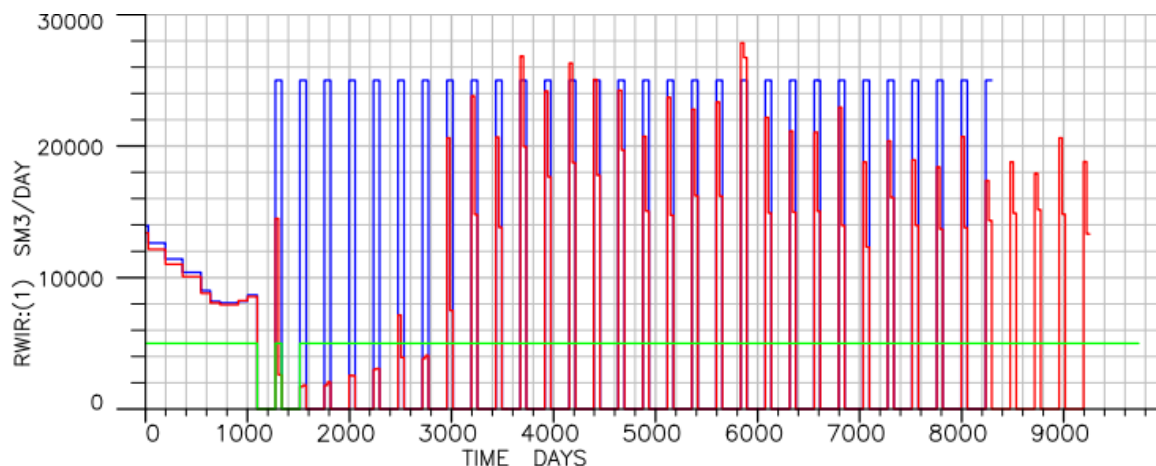


Figure 67-Water injection rates in WAG region (light oil)

3.5.4 WAG ratio

WAG ratio is the ratio between the volumes of injection water to the volume of injected gas (CO₂), at reservoir conditions. Two simulations have been run and compared to the reference case. The observed results indicate that oil recovery increases with decreasing WAG ratio as shown in Fig 55. These results and observations agree with past studies [52] [53] [46] on the same effect. They all have reached a conclusion that an unnecessary high water amount in WAG ratios delays the CO₂ from contacting and displacing the reservoir oil by being an obstacle between them. This will result in a delay in recovery, as shown in (Fig 69). However, this effect has a limit after which the relation is reversed and becomes more like a normal CO₂ continuous injection.

The effect was nearly the same with light oil and medium oil. In the shown figure, the referred delay started at the moment of starting the EOR process. The recovery factor difference is maximum at a time of about 2,600 days, and it has reached a value of 0.25 of oil in place difference between the highest and lowest recoveries. This value is compensated, in the 3:1 ratio case, after 1,400 additional days.

Table 11- Key legend for figure 69

1 : 6 (ref. case)	Blue
1 : 10	Red
3 : 1	Green

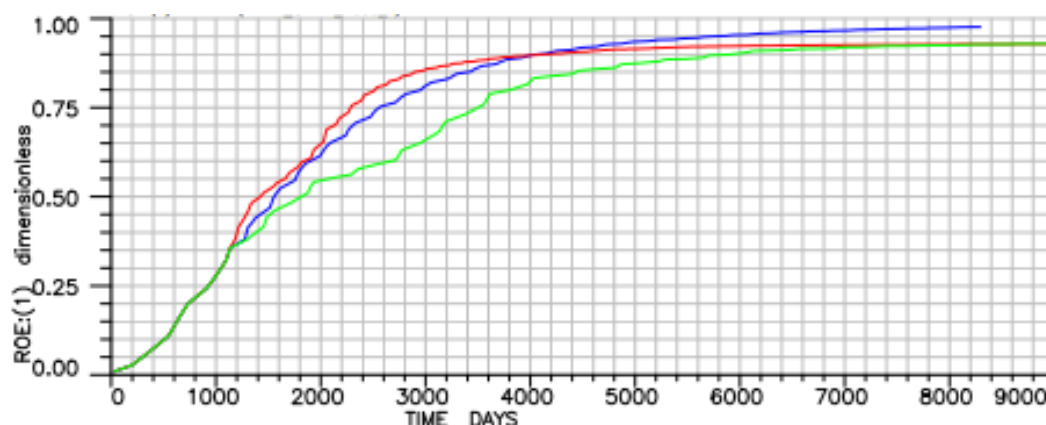


Figure 68- Recovery factor in WAG region with different WAG ratios (light oil)

3.5.5 Effect of total CO₂ injected volume

To study the effect of this parameter, the CO₂ injection rate was chosen to be the modified value, and 10 years of production is chosen to be the time at which comparison will be made amongst recoveries and total injected volumes.

Four simulation runs have been performed and compared with the reference case. Two representative groups of results and the base case are presented in (Fig 70). The figure shows the recovery factors and total injected CO₂ for three different light oil cases with three different CO₂ injection rates.

The highest recovery factor case corresponds to a total CO₂ injection of 2 HCPV (hydrocarbon pore volume), the next corresponds to 1.3 HCPV and the lowest recovery corresponds to about 0.6 HCPV, where HCPV of CO₂ is calculated by multiplying its total injected volume by the formation volume factor of CO₂, which is around 0.002 [54].

As observed, at 10 years of production, the recovery factor increases with increasing the total injected amount of CO₂, however, the rate of this increment decreases with higher total injected volumes. The difference in recoveries of the 2 HCPV curve and 1.3 HCPV is lower than the difference in recoveries of the 0.6 HCPV curve and 1.3 HCPV curve. These results are consistent with previous works on the same topic [55] [46]. They found a significant increment in oil recovery at a certain time with increasing the total injected volume, however, after a certain value of total injected CO₂ then no additional recovery was obtained. This could be explained as follows, as the amount of injected CO₂ increases, processes stimulated by CO₂-oil interactions increases, like oil density and viscosity reduction, oil vaporization, and oil swelling, while this results in an enhancement of oil production. The decrease in the incremental rate of recovery factor may be a result of the reduction in oil in place [46].

Table 12- Key legend for figure 70

300,000 Sm ³ /d (Reference case)	Blue
100,000 Sm ³ /d	Green
500,000 Sm ³ /d	Red

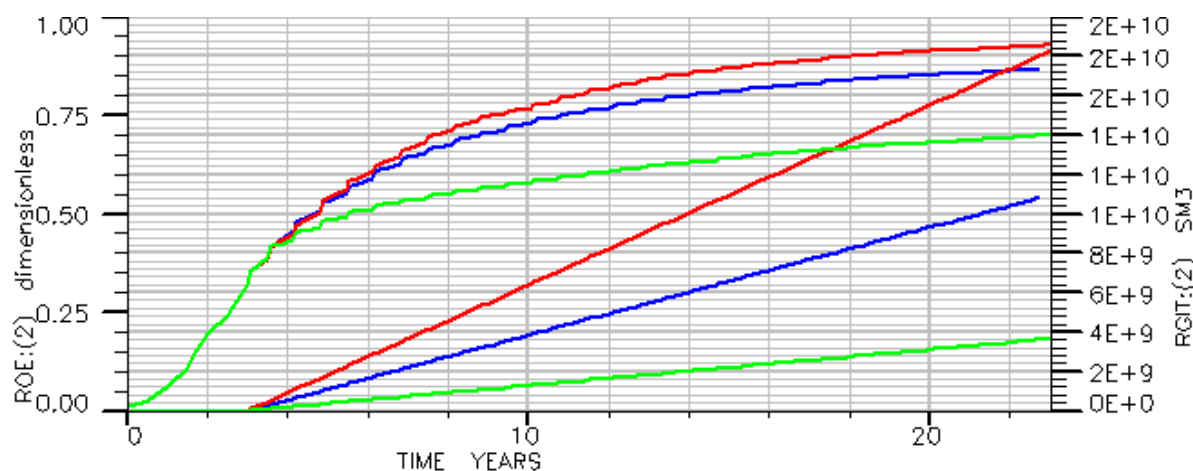


Figure 69- Effect of total injected volume of CO2 on the recovery factor, continuous CO2 region (light oil)

4 Conclusion

In this study, a comprehensive literature review has been presented, covering what was believed to be essential for better understanding the topic of miscible CO₂-EOR process. Besides, an oil reservoir numerical model was built and characterized, with the aid of an advanced commercial software package. Then a miscible CO₂-EOR process was designed and applied to the mentioned model. A sensitivity analysis targeted the study of different deterministic factors that are critical for a project's success.

As previously discussed in the literature review, displacing oil with CO₂ can be done according to a miscible or immiscible process. Generally, an immiscible process is chosen in the case of shallow reservoirs or heavy oils, other than that, miscible injection is preferred because of high displacement efficiency. The miscible CO₂-oil displacement process involves oil swelling, oil viscosity and density reduction, and oil vaporization. These sub-processes occur due to a condensing-vaporizing mechanism of miscibility development. In this process, CO₂ condenses into oil, and oil light and intermediate components vaporize into CO₂ creating a transition zone between the two phases that results in a reduction or, in ideal cases, in total elimination of viscous and capillary forces.

For a successful reservoir simulation and field development, it is essential to understand the way that injected fluids, CO₂ or water, will interact with the reservoir oil and rock. Defining parameters like diffusion coefficient, relative permeabilities, and capillary pressure will be critical in the history-matching stage.

In this work, a sensitivity analysis was done to study five important design parameters. The analysis, supported by previous work, has shown which criticalities are in the process of CO₂-EOR.

Sensitivities on flood patterns have shown that, for both WAG and continuous CO₂ injection with light and medium oils, the recovery factor decreases with increasing the designed influence area of an injection well, but at a certain point the relationship is inverted. The first relation is due to the inability of the well to provide the target amount of CO₂ to cover such a large area. While the inversion in this relation is because wells are sufficiently away from one another, and the pore pressure created does not hinder injection, this was referred to as higher injectivity.

The influence of the CO₂ injection rate was also studied and analyzed. In all the tested scenarios, the results of the sensitivity analysis indicate a remarkable increase in the EOR when increasing the injection rate. These results are representative and consistent with the previous investigations. The reason for this oil production enhancement is related to the increase in pressure as a result of more CO₂ molecules that cover more voids and gets in touch with more oil. The recommendation provided could be to increase the injection rate, however, economic limitations for CO₂ cost and injection facilities cost should be considered in addition to the damages that may develop in the cap rock.

Water injection rate effects on the WAG injection process was also investigated. Some observations were made based on the sensitivity analysis results and they agree with past studies. The influence of the water injection rate on oil recovery was not as important as the CO₂ injection rate influence because the CO₂ displaces oil in a miscible displacement process which is more effective in terms of oil recovery. However, it was observed that water injectivity reduces when increasing the water injection rate. This reduction in injectivity is less severe in the water alternating CO₂ process.

The effect of the WAG ratio was also examined by varying the ratio in the sensitivity runs. The reported results indicate a delay in oil recovery when increasing this ratio. However, this relation has a certain limit after which it is reversed and results become closer to continuous CO₂ injection results, which in turn has a lower recovery. This was supported by several previous results on the same topic.

Finally, the influence of the total injected volume of CO₂ in terms of Hydrocarbon Pore Volume on oil recovery was studied. A certain time was chosen for comparison (10 years) and oil recovery results were plotted with the corresponding CO₂ total injected volume. A proportional nonlinear relation was obtained. As the total injected volume of CO₂ increases, oil recovery increases until a certain limit after which there is no additional recovery that will result from further injection. The proportionality was explained by the enhancement of the recovery mechanisms when increasing the CO₂ amount, while the gradual dissipation of this influence is explained by a much less oil that remained in the reservoir.

5 References

- [1] Green D.W. & Willhite. G.P., 1998, "Enhanced Oil Recovery", SPE Text Book Series Vol. 6 Richardson Texas,
- [2] Brigham W.E. & Reed P.W., 1961, "Experiments on Mixing During Miscible Displacement in Porous Media" SPE J., SPE-1430-G. <https://doi.org/10.2118/1430-G>
- [3] Perkins T.K. & Johnston O.C., 1963, "A Review of Diffusion and Dispersion in Porous Media", SPE J., SPE-480-PA. <https://doi.org/10.2118/480-PA>
- [4] Schwartz C.E. & Smith J.M., 1953, "Flow Distribution in Packed Beds", Ind. Eng. Prog. Vol. 45, 1209. <https://doi.org/10.1021/ie50522a025>
- [5] Raimondi P. & Gardner G.H., 1959, "Effect of Pore Structure and Molecular Diffusion on the Mixing of Miscible Liquids Flowing in Porous Media", Preprint 43 presented at AIChE-SPE Joint Symposium, San Francisco, Cal. <https://doi.org/10.1029/WR026i001p00087>
- [6] Kasraie M. & Farouq S.M., 1984, "Role of Immobile Phase Saturations in Tertiary Oil Recovery", SPE Enhanced Oil Recovery Symposium, Tulsa, Oklahoma. <https://doi.org/10.2118/12635-MS>
- [7] Aris R., 1959, "The Longitudinal Diffusion Coefficient in Flow Through a Tube with Stagnant Pockets", Chem. Eng. Sci. Vol. 11, 194. [https://doi.org/10.1016/0009-2509\(59\)80086-5](https://doi.org/10.1016/0009-2509(59)80086-5)
- [8] Blackwell R.J., 1962, "Laboratory Studies of Microscopic Dispersion Phenomena", SPE J. SPE-1483-G. <https://doi.org/10.2118/1483-G>
- [9] Gratton L.C. & Fraser H.J., 1935, "Systematic Packing of Spheres-With Particular Relation to Porosity and Permeability", Journal of Geology 785. <https://doi.org/10.1086/624386>
- [10] Fahien R.W. & Smith J.M., 1955, "Mass Transfer in Packed Beds", AIChE Jour. Vol. 1, 28. <https://doi.org/10.1002/aic.690010104>
- [11] Keable D. & Jones A., 2021, "The Effect of Viscosity Ratio and Peclet Number on Miscible Viscous Fingering in a Hele-Shaw Cell: A Combined Numerical and Experimental Study", arXiv.org. <https://doi.org/10.48550/arXiv.2111.06548>
- [12] Tarek Ahmed, 2010, "Reservoir Engineering Handbook", Vol. 4.
- [13] Ghoojani E. & Bolouri S.H., 2011, "Experimental Study of CO₂-EOR and N₂-EOR with Focus on Relative Permeability Effect" ISSN: 2157-7463 JPEB, an open access journal. <https://doi.org/10.4172/2157-7463.1000106>
- [14] Mangalsingh D. & Jagai T., 1996, "A Laboratory Investigation of the Carbon Dioxide Immiscible Process", SPE Latin America/Caribbean Petroleum Engineering Conference, <https://doi.org/10.2118/36134-MS>
- [15] Srivastava R.K. & Huang S., 1997, "Comparative Effectiveness of CO₂, Produced Gas, and Flue Gas for Enhanced Medium Oil Recovery", SPE 37558, International Thermal Operations and Medium Oil Symposium, California. <https://doi.org/10.2118/56857-PA>
- [16] Simon R. & Graue D.J., 1965, "Generalized Correlations for Predicting Solubility, Swelling and Viscosity Behavior of CO₂-Crude Oil System." JPT 23: 102-106. <https://doi.org/10.2118/917-PA>
- [17] McDougall S.R. & Salina P.A., 1997, "The Effect of Interfacial Tension upon Gas-Oil Relative Permeability Measurements: Interpretation Using Pore- Scale Models". SPE 38920, SPE Annual Technical Conference and Exhibition, San Antonio, Texas. <https://doi.org/10.2118/38920-MS>
- [18] du Prey L., 1973, "Factors Affecting Liquid-Liquid Relative Permeabilities of a Consolidated Porous Media", JPT 39-47. <https://doi.org/10.2118/3039-PA>
- [19] Moodie N. & Ampomah W., 2021, "Quantitative Analysis of the Influence of Capillary Pressure on Geologic Carbon Storage Forecasts Case Study: CO₂-EOR in the Anadarko Basin,

- Texas”, *International Journal of Greenhouse Gas Control*.
<https://doi.org/10.1016/j.ijggc.2021.103373>
- [20] Wang Y. & Orr F.M. Jr., 2000, "Calculation of minimum miscibility pressure", SPE100E Improved Oil Recovery Symposium, Tulsa, Oklahoma. [https://doi.org/10.1016/S0920-4105\(00\)00059-0](https://doi.org/10.1016/S0920-4105(00)00059-0)
- [21] Hutchinson C.A. Jr. & Braun P.H., 1961, "Phase relations of miscible displacement in oil recovery", *AICHE J.*, 64–72. <https://doi.org/10.1002/aic.690070117>
- [22] Benham A.L. & Dowden, W.E., 1959, "Miscible fluid displacement - prediction of miscibility", *Trans. AIME* 216, 388–398. <https://doi.org/10.2118/1484-G>
- [23] Metcalfe R.S. & Fussell D.D., 1973, "A multicell equilibrium separation method for the study of multiple contact miscibility in rich gas drives", *SPEJ, Soc. Pet. Eng. J.*
<https://doi.org/10.2118/3995-PA>
- [24] Kuo S.S., 1985, "Prediction of miscibility for the enriched gas drive process", SPE 14152, SPE Ann. Tech. Conf., Las Vegas, NV. <https://doi.org/10.2118/14152-MS>
- [25] Luks K.D. & Turek E.A., 1987, "Calculation of minimum miscibility pressure", *SPE Reservoir Eng.*, 501–506. [https://doi.org/10.1016/0920-4105\(93\)90008-3](https://doi.org/10.1016/0920-4105(93)90008-3)
- [26] Nouar A. & Flock D.L., 1986, "Prediction of the minimum miscibility pressures of a vaporizing gas drive", SPE 15075, 56th California Regional Meeting, Oakland, CA.
<https://doi.org/10.2118/15075-PA>
- [27] Zick A.A., 1986, "A combined condensing vaporizing mechanism in the displacement of oil by enriched gas", SPE 15493, SPE Ann. Tech. Conf., New Orleans, LA.
<https://doi.org/10.2118/15493-MS>
- [28] Stalkup F.I., 1987, "Displacement behavior of the condensing vaporizing gas drive process", SPE 16715, SPE Ann. Tech. Conf., Dallas, TX. <https://doi.org/10.2118/16715-MS>
- [29] Jensen F. & Michelsen M.L., 1990, "Calculation of first contact and multiple contact minimum miscibility pressures", *In Situ* 14 1, 1–17. [https://doi.org/10.1016/S0378-3812\(98\)00414-2](https://doi.org/10.1016/S0378-3812(98)00414-2)
- [30] Monroe W.W. & Silva M.K., 1990, "Composition paths in four-component systems: effect of dissolved methane on 1D CO flood performance", *SPE Reservoir 2 Eng.* 5, 423–432.
<https://doi.org/10.2118/16712-PA>
- [31] Orr, F.M. Jr. & Silva M.K., 1987, "Effect of oil composition on minimum miscibility pressure — Part 2: Correlation", *SPE Reservoir Eng.* 2, 479–491. <https://doi.org/10.2118/14150-PA>
- [32] Johns R.T. & Dindoruk B., 1993, "Analytical theory of combined condensing/vaporizing gas drives", *SPE Adv. Tech. Ser.* 237–16. <https://doi.org/10.2118/24112-PA>
- [33] Johns R.T. & Orr F.M. Jr., 1996, "Miscible gas displacement of multicomponent oils", *SPEJ, Soc. Pet. Eng. J.* 1139–50. <https://doi.org/10.2118/30798-PA>
- [34] Wang Y. & Orr F.M. Jr., 1997, "Analytical calculation of minimum miscibility pressure. Fluid Phase Equilibrium", 139, 101–124. [https://doi.org/10.1016/S0378-3812\(97\)00179-9](https://doi.org/10.1016/S0378-3812(97)00179-9)
- [35] Wang Y. & Douglas G., 2000, "Analytical Calculation of Minimum Miscibility Pressure: Comprehensive Testing and Its Application in a Quantitative Analysis of the Effect of Numerical Dispersion for Different Miscibility Development Mechanisms" Improved Oil Recovery Symposium, Tulsa, Oklahoma. <https://doi.org/10.2118/59378-MS>
- [36] Yuan H. & Johns R.T., 2005, "Simplified Method for Calculation of Minimum Miscibility Pressure or Enrichment", *SPE J.* 10 (04): 416–425. <https://doi.org/10.2118/77381-PA>
- [37] Shokrollahi A. & Arabloo M., 2013, "Intelligent model for prediction of CO₂ – Reservoir oil minimum miscibility pressure" *Fuel* 112, 375-384. <https://doi.org/10.1016/j.fuel.2013.04.036>
- [38] Yuan H. & Johns R.T., 2004, "Improved MMP Correlations for CO₂ Floods Using Analytical Gas Flooding Theory", SPE/DOE Symposium on Improved Oil Recovery, Tulsa, Oklahoma.
<https://doi.org/10.2118/89359-MS>

- [39] Echeverry J.S.L., 2007, "A modified temperature dependence for the Peng–Robinson equation of state", *Fluid Phase Equilibria* 447, 39-71.
<https://doi.org/10.1016/j.fluid.2017.05.007>
- [40] IEA report, 2021, "World Energy Outlook. <http://www.worldenergyoutlook.org/S>.
- [41] IEA report, 2021, "Net Zero by 2050", 4th revision. <https://www.iea.org/topics/net-zero-emissions>
- [42] Hook M. & Hirsch R., 2009, "Giant oil field decline rates and their influence on world oil production", *Energy Policy*, 37, 2262–2272. <https://doi.org/10.1016/j.enpol.2009.02.020>
- [43] Kuuskraa V.A. & Koperna G.J., 2006, "Evaluating the Potential for “Game Changer” Improvements in Oil Recovery Efficiency Using CO2 EOR", U.S. Department of Energy, Washington, DC, USA. <https://adv-res.com/>
- [44] IEA report, 2022, "Oil Information". <https://www.iea.org/reports/oil-information-overview>
- [45] Kulkarni M.M., 2003, “Immiscible and Miscible Gas-Oil Displacements in Porous Media” Master’s Thesis, Louisiana State University, Baton Rouge, LA, USA.
https://digitalcommons.lsu.edu/gradschool_theses/259/
- [46] Perera M. S. A. & Gamage R. P., 2016, "A Review of CO2 - Enhanced Oil Recovery with a Simulated Sensitivity Analysis", *Energies*, 9(7), 481. <https://doi.org/10.3390/en9070481>
- [47] Bush Convention Center, Midland, Texas, 2020, "A Brief History of CO2 EOR, New Developments and Reservoir Technologies for CO2 EOR in Conjunction with Carbon Capture, Utilization and Storage (CCUS)" 26th Annual CO2 Conference.
<https://www.co2conference.net>
- [48] Meyer J.P. "Summary of Carbon Dioxide Enhanced Oil Recovery (CO2-EOR) Injection Well Technology”, API background report. <https://www.api.org>
- [49] Gozalpour F. & Ren S.R., 2005, "CO2-EOR and storage in oil reservoirs", *Oil & Gas Sci. Technol.* 60, 537–546. <https://doi.org/10.2516/ogst:2005036>
- [50] Liu K. & Clennell B., 2013, "Laboratory Investigation of Factors Affecting CO2 Enhanced Oil and Gas Recovery" SPE Enhanced Oil Recovery Conference, Kuala Lumpur, Malaysia.
<https://doi.org/10.2118/165270-MS>
- [51] Coats K.H. & Smart G.T., 1986, “Application of a Regression-Based EOS PVT Program to Laboratory Data”, *SPE Reservoir Engineering*, 1(3), 277–299. <https://doi.org/10.2118/11197-PA>
- [52] Thomas S., 2008, "Enhanced oil recovery-an overview", *Oil Gas Sci. Tech. Rev. IFP* 63, 9–19. <https://doi.org/10.2516/ogst:2007060>
- [53] Ghedan S., 2009, "Global laboratory experience of CO2-EOR flooding", *SPE/EAGE Res. Char. & Sim. Con.*, Abu Dhabi, United Arab Emirates, 19–21. <https://doi.org/10.2118/125581-MS>
- [54] Bech N. & Larsen M., 2005, "Storage of CO2 in the Havnsø aquifer - a simulation study", A CO2STORE contribution, Geological Survey of Denmark and Greenland report.
- [55] Comberiat J.R. & Zammerilli A.M., 1982, "Effects of Petroleum-Reservoir Conditions on Oil Recovery by Carbon Dioxide Injection", U.S. Department of Energy: Morgantown, WV, USA. DOE/METC/TPR-83-4 (DE83008455).
- [56] Yang D. & Song C., 2015, “Performance evaluation of injectivity for water-alternating-CO2 processes in tight oil formations” *Fuel*, vol. 139, 292-300.
<https://doi.org/10.1016/j.fuel.2014.08.033>
- [57] Tanner C.S. & Baxley P.T., 1992, "Production Performance of the Wasson Denver Unit CO2 Flood", *SPE/DOE Enhanced Oil Recovery Symposium*, Tulsa, Oklahoma.
<https://doi.org/10.2118/24156-MS>

- [58] Kim T. H. & Crane D.J., 2018, "Infill Well Location Selection Procedures in Lost Hills Using Machine Learning", SPE Western Regional Meeting, Garden Grove, California. <https://doi.org/10.2118/190101-MS>
- [59] Kaita A.Y. & Ogolo O., 2020, "Study of the impact of injection parameters on the performance of miscible sour gas injection for enhanced oil recovery" *Journal of Petroleum Exploration and Production Technology*, 10 (1575-1589). <https://doi.org/10.1007/s13202-019-00793-4>
- [60] Ghoojani E. & Bolouri S.H., 2012, "Numerical and Analytical Optimization of Injection Rate During CO₂-EOR and-Sequestration Processes" *Carbon Management Technology Conference*, Orlando, Florida. <https://doi.org/10.7122/150157-MS>
- [61] Huang E.T.S. & Holm L.W., 1988, "Effect of WAG Injection and Rock Wettability on Oil Recovery During CO₂ Flooding" *SPE Reservoir Engineering*, 3(1), 119–129. <https://doi.org/10.2118/15491-PA>
- [62] Ghahfarokhi R.Z., Pennell S., 2016, "Overview of CO₂ Injection and WAG Sensitivity in SACROC", *SPE Improved Oil Recovery Conference*, Tulsa, Oklahoma. <https://doi.org/10.2118/179569-MS>
- [63] Ghedan S.G., 2009, "Global Laboratory Experience of CO₂-EOR Flooding" *SPE/EAGE Reservoir Characterization and Simulation Conference*, Abu Dhabi. <https://doi.org/10.2118/125581-MS>
- [64] Panjalizadeh H. & Alizadeh A., 2015, "Optimization of the WAG Injection Process", *Petroleum Science and Technology*, 33(3), 294-301. <https://doi.org/10.1080/10916466.2014.956897>
- [65] Saman A.A. & Curtis B., 2014, "North Cross Devonian Unit - A Mature Continuous CO₂ Flood Beyond 200% HCPV Injection", *SPE Annual Technical Conference and Exhibition*, Amsterdam. <https://doi.org/10.2118/170653-MS>
- [66] Killough J.E. & Kossack C.A., 1987, "Fifth Comparative Solution Project: Evaluation of Miscible Flood Simulators", *SPE Symposium on Reservoir Simulation*, San Antonio, Texas. <https://doi.org/10.2118/16000-MS>
- [67] Shaw J. & Bachu S., 2002, "Screening, Evaluation, and Ranking of Oil Reservoirs Suitable for CO₂-Flood EOR and Carbon Dioxide Sequestration" *Journal of Canadian Petroleum Technology*, 41(9). <https://doi.org/10.2118/02-09-05>
- [68] Ozan P., 2005, "Basin oriented strategies for CO₂ enhanced oil recovery: and Oklahoma. Onshore Gulf Coast" A report for the US Department of Energy, by Advanced Resources International. <https://netl.doe.gov/oil-gas/oil-recovery>
- [69] Suleimanov B.A. & Ismayilov F.S., 2016, "Selection methodology for screening evaluation of EOR methods", *Petroleum Science and Technology*, 34(10), 961–970. <https://doi.org/10.1080/10916466.2015.1107849>.
- [70] Taber J.J. & Martin F.D., 1997, "EOR Screening Criteria Revisited - Part 1: Introduction to Screening Criteria and Enhanced Recovery Field Projects" *SPE Reservoir Engineering*, 12(3), 189–198. <https://doi.org/10.2118/35385-PA>
- [71] Bachu A., 2016, "Identification of oil reservoirs suitable for CO₂-EOR and CO₂ storage (CCUS) using reserves databases, with application to Alberta, Canada", *International Journal of Greenhouse Gas Control*, 44, 152–165. <https://doi.org/10.1016/j.ijggc.2015.11.013>